
Chandan Pandey

# Simulation-Based Grid Code Compliance Testing for Mega Watt Charging Systems

School of Technology and Innovation
Master of Science in Technology
Master's Programme in Electrical Engineering

Vaasa 2026

**UNIVERSITY OF VAASA**
**School of Technology and Innovation**

| | |
|---|---|
| **Author:** | Chandan Pandey |
| **Title of the thesis:** | Simulation-Based Grid Code Compliance Testing for Mega Watt Charging Systems |
| **Degree:** | Master of Science in Technology |
| **Degree Programme:** | Smart Energy |
| **Supervisor at University of Mons:** | Zacharie De Greve |
| **Second Academic Supervisor at UWASA:** | Mustafa Alrayah Hassan Ibraheem |
| **Partner Supervisor** | Panu Lauttamus |
| **Instructor:** | Kamran Khan |
| **Year:** | 2026 **Pages:** 115 |


**ABSTRACT:**

Electrification of heavy-duty vehicles is pushing the demand for megawatt-level chargers (MCS) capable of delivering high-power loads in an efficient manner. The integration of such high-powered systems into the electric grid poses concerns regarding power quality and reliability issues due to the poor grid condition in many locations. The current research investigates the Grid-Integrated MCS Validation Framework (GMVF) under the project called Grid code Compliance by Simulation (GCCS) for evaluating the performance of megawatt EV chargers under realistic network conditions.

A comprehensive simulation model of megawatt class charging system was designed using MATLAB/Simulink software, which includes AC-DC interface converter for connection to the utility grid, isolated DC/DC converter, and battery charger following CC-CV control strategy. Simulations were conducted under different grid conditions, ranging from strong to moderate and weak grids, especially focusing on PCC performance. To be consistent with industry standards, testing according to EN 50549-2 standard procedures was carried out, including LVRT capability, OVRT capability, steady-state deviation of voltages up to ±10%, and off-nominal frequency operation of 49 Hz. Protection and operation were modelled to meet IEC 61851-23-3 guidelines for high power DC charging systems.

From the findings, it can be concluded that the system works well at megawatt-scale operations, even in difficult circumstances like variation in voltage and frequency of the grid. In the ride-through scenarios, the charger stays connected and is able to recover well, thereby fulfilling grid code requirements for continuous operation. Increased harmonic distortion and higher system stress were observed under weak-grid conditions, highlighting the importance of grid strength for stable megawatt charging system operation. Influence of converter topology on system performance for varying grid condition was identified. Two-level inverters were found better in strong grids, but limitations were observed when the grid is weak. Three-level inverters, by contrast, deliver better harmonic performance and stability under challenging conditions, making them more suitable for weak grids. The findings also highlight the importance of site-based grid evaluation prior to the deployment of megawatt charging systems. Reliable operation of chargers without violating standards is more important than obtaining perfect waveforms. This study shows that it is important to assess the characteristics of grids before designing and configuring the charging system with appropriate topology and protection measures. The proposed framework provides a practical simulation-based approach to evaluate grid-compliant megawatt charging stations prior to deployment.

**KEYWORDS:** Megawatt Charging System (MCS), Grid Code Compliance by Simulation (GCCS), Weak Grid, Power Quality, EN 50549-2, IEC 61851-23-3, Converter Topology, EV Charging

## Acknowledgements

I would like to express my sincere gratitude to my main supervisor, Professor Zacharie De Greve from UMONS (Belgium), for his guidance, feedback, and support in academics. He has had a great influence on this thesis because of his expertise and systematic way of thinking.

Furthermore, I would like to thank Project Head Professor Kimmo Kauhaniemi of the GCCS project of the University of Vaasa for giving me the chance to contribute to the research through this thesis. His leadership and vision have played a significant role in making this thesis what it is today.

Sincerely, I am very grateful for the support of my assistant supervisor, Dr. Mustafa Alrayah Hassan from UWASA (Finland), for all the guidance he gave me and our numerous discussions about the project throughout the thesis development. His understanding of converter interactions is marvelous.

I would also like to express my sincere gratitude to Kamran Khan for his support and practical perspective which contributed positively to the development of this thesis.

I am grateful for the financial support from Business Finland in funding the GCCS project. Through the project, the University of Vaasa worked together with various industry partners, which supported applied research in megawatt charging systems.

I would also like to thank my industrial partner Kempower for its contribution to the research through practical insight into industry problems. Due to industrial collaboration associated with this work, certain implementation details remain confidential.

I wish to extend my gratitude to my parents, friends, and the entire team of researchers in the GCCS project who have constantly motivated, supported, and trusted me throughout the process.

## Contents

## Figures

## Tables

## Abbreviations

| Abbreviation | Full Form |
|---|---|
| **AC** | Alternating Current |
| **AFE** | Active Front-End |
| **Ah** | Ampere-hour |
| **BESS** | Battery Energy Storage System |
| **CC** | Constant Current |
| **CC–CV** | Constant Current–Constant Voltage |
| **CV** | Constant Voltage |
| **DC** | Direct Current |
| **DSOGI** | Dual Second-Order Generalized Integrator |
| **EMC** | Electromagnetic Compatibility |
| **EN** | European Norm |
| **EV** | Electric Vehicle |
| **EVSE** | Electric Vehicle Supply Equipment |
| **EVGI** | Electric Vehicle Grid Integration |
| **FRT** | Fault Ride-Through |
| **GCCS** | Grid Code Compliance by Simulation |
| **GMVF** | Grid-Integrated MCS Validation Framework (GMVF) |
| **Hz** | Hertz |
| **Ibat** | Battery Current |
| **Icc** | Constant Current Reference |
| **Idc** | Direct Current (DC Current) |
| **IEC** | International Electrotechnical Commission |
| **IEEE** | Institute of Electrical and Electronics Engineers |
| **kHz** | Kilohertz |
| **kWh** | Killo Watt Hour |
| **KPI** | Key Performance Indicator |
| **LCL** | Inductor–Capacitor–Inductor Filter |
| **LVRT** | Low-Voltage Ride-Through |
| **MCS** | Megawatt Charging System |
| **MV** | Medium Voltage |
| **NPC** | Neutral Point Clamped |
| **OCV** | Open Circuit Voltage |
| **OVRT** | Overvoltage Ride-Through |
| **PCC** | Point of Common Coupling |
| **PLL** | Phase-Locked Loop |
| **PWM** | Pulse Width Modulation |
| **RMS** | Root Mean Square |
| **SCR** | Short-Circuit Ratio |
| **SOC** | State of Charge |
| **THD** | Total Harmonic Distortion |
| **Ts** | Sampling Time |
| **Vbat** | Battery Voltage |

| | |
|---|---|
| **Vdc** | DC-Link Voltage |
| **VLL** | Line-to-Line Voltage |
| **VSC** | Voltage Source Converter |
| **VSM** | Virtual Synchronous Machine |
| **V2G** | Vehicle-to-Grid |
| **X/R** | Reactance-to-Resistance Ratio |

# 1 Introduction

The purpose of this chapter is to provide an understanding of the background and reasoning behind the analysis of mega-watt electric vehicle charger systems. The chapter also explains the issues that will be considered, gaps in current literature, and objectives pursued in this thesis alongside the scope of work considered for research.

## 1.1 Background and Motivation

Electromobility is evolving rapidly, particularly for those applications requiring high energy consumption, such as heavy trucks used for intercity and intercontinental cargo transportation. As evident from **Figure 1-1**, electric truck sales have increased drastically in recent years in various regions, in fact by 80% in year 2024 as per International Energy Agency (IEA, 2025). The rapid development and increasing popularity of electric trucks signify a move towards electric cargo transportation. High-power charging solutions are required because electric trucks have high battery capacity and require fast charging. Thus, today megawatt charging solutions are necessary for effective usage of heavy-duty electric trucks. However, integration of such high-capacity charging stations into the existing power system faces numerous issues related to grid interaction, power quality, system reliability and grid code requirements (Acharige et al., 2023).

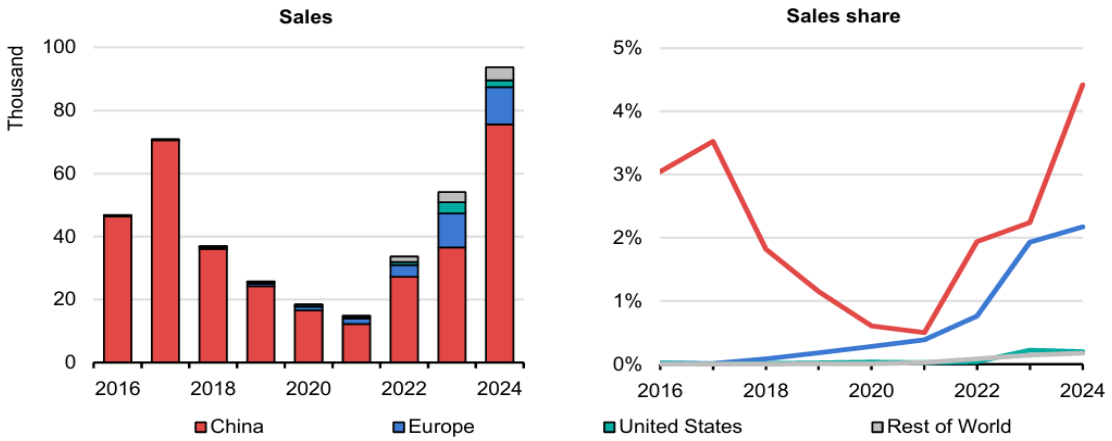


**Figure 1-1**: Global electric truck sales and sales share by region (2016–2024), illustrating the rapid growth and regional distribution of heavy-duty vehicle electrification. Source: International Energy Agency (IEA), Global EV Outlook 2025.

Firstly, MCS is a technology that interacts with the grid and acts as an interface between the grid and the charger, impacting the voltage profiles, waveforms of currents, and overall stability of the distribution network. As the charging infrastructures evolve and the charging stations become larger, the impact of charging system on the grid needs to be considered thoroughly. Hence, a complete architecture for the power grid that includes grid control, protection, and converter coordination becomes important. The complete architecture considered for simulation-based evaluation of grid compliance in this work is given in **Figure 1-2**.

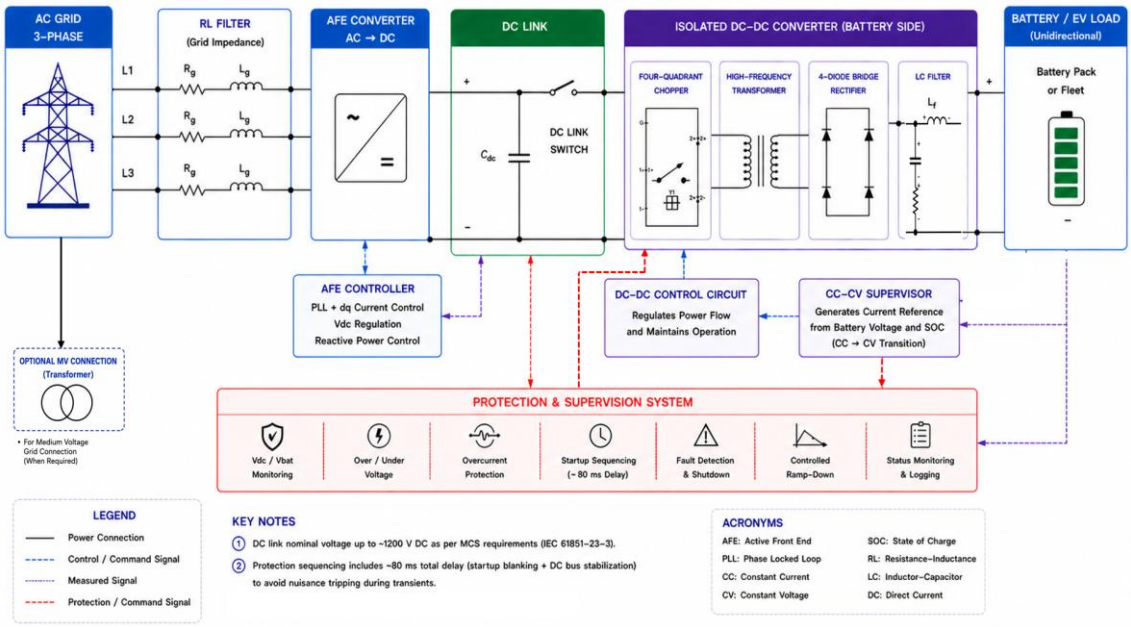


**Figure 1-2**: System-level architecture of the proposed megawatt-scale EV charging system used for GMVF-based grid compliance and power quality assessment.

An important issue connected to this question is how such systems behave in a case where the quality of the grid is relatively poor. Specifically, weak grids with low short-circuit ratio limit their capability to accommodate changes in the network and make it more sensitive to voltage fluctuations, dynamic instability and harmonic distortion. Therefore, it is essential to understand and validate the performance of megawatt charging systems under varying grid conditions for successful deployment.

Grid Connection Standards like EN 50549-2 include parameters for the tolerance of voltage and frequency, which include ride-through requirements. Likewise, IEC 61851-23-3

includes requirements for operations and safety regarding high power charging systems. Nevertheless, it is often not feasible to test such requirements on-site owing to issues related to costs and safety measures.

As an alternative, simulation methods can be used, allowing the testing of grid connected devices based on software. For instance, the Grid Code Certification through Simulation method uses software techniques such as Software in the Loop to test various aspects of grid connected devices. Therefore, this approach allows detailed analysis of system behavior across a wide range of operating scenarios, including fault conditions and grid disturbances.

## 1.2 Problem Statement and Challenges

Despite the improvements made in EV chargers' technologies, there are still some problems related to the reliable and grid-conform operation of megawatt chargers:

- **Dependence on grid strength:** The functioning of converters depends largely on the parameters of the grid, especially on the weak grid with low SCR values, which leads to higher instability and sensitivity to the change in control strategies.
- **Issues with the power quality:** Large power converters might be sources of harmonic distortions and voltage deviations at the point of common coupling (PCC).
- **Problems with dynamic grid phenomena:** Voltage dips (LVRT), voltage swells (OVRT), and frequency deviations must be handled by converters while maintaining their stable work during operation.
- **Converter topology selection:** The appropriateness of various converters topologies (2-level and 3-level inverters) with regard to grid conditions is not known yet in case of megawatt scales.
- **Coordination issues**: Due to the transitory processes during operation at high power levels, the protection mechanism may trip unnecessarily in case mechanisms are not properly synchronized with converter dynamics.

These challenges highlight the need for a system-level evaluation methodology that captures both grid conditions and converter behavior.

## 1.3 Research Gap

The current state of research on EV charging stations mainly focuses on low-power levels or operating systems in the presence of ideal grid conditions. While some papers may focus on power quality and converter control, there is a lack of systematic studies concerning:

- The influence of grid strength and converter configuration on the operation of megawatt-level charging stations.
- The performance of charging stations when subjected to standard grid disturbances like LVRT, OVRT, and frequency variations.
- The use of simulation tools to verify compliance with grid codes for megawatt-level charging stations.
- Translating simulation results into practical recommendations for engineering implementation.

Furthermore, there is an evident lack of work that bridges the gap between simulation tools and real world or practical system design, particularly for grid-connected megawatt charging systems.

## 1.4 Objective of Thesis

The primary objective of this thesis is to develop and apply a simulation-based framework for evaluating grid code compliance and performance of a megawatt-scale EV charging system.

**The specific objectives are as follows:**

1. To create a simulation model for the megawatt charging system, considering the grid connected AC-DC converter, isolated DC-DC converter stage and battery charging stage with CC-CV control.
2. To study the behavior of the system with various grid operating conditions like strong grid, medium grid and weak grid operation.

3. To analyze the behavior of the system under various standard grid disturbances such as LVRT, OVRT, ±10% grid disturbance voltage and grid disturbance in frequency.
4. To study KPIs such as THD, DC link ripple voltage, etc.,
5. To analyze various types of converter stages to check their viability with varying grid operation.
6. To draw practical conclusions useful for designing megawatt EV charging systems.

## 1.5 Scope of Work

In this thesis, the simulation approach is used for analysis of a megawatt-class charger in terms of power quality and grid interaction at point of common coupling (PCC), based on MATLAB/Simulink software within a Software-in-the-Loop (SIL) approach.

While in general the overall system comprises multiple chargers connected at PCC, but here the purpose of this research is focused on one particular charger to gain insight into the operation of the system itself and the interconnection with the grid. The results gained in this thesis are meant to be relevant for systems of higher scales.

**Scope of this thesis includes the following aspects:**

- Grid interaction and power quality analysis at the point of common coupling (PCC)
- System analysis under specific scenarios of grid disturbances
- Converter performance analysis and its stability

**The scope of this research excludes the following topics:**

- Hardware design and experimental work
- Modeling and analysis of EMC issues
- Network simulations beyond local PCC

## 1.6 Organization of The Thesis

The subsequent chapters of this thesis are organized as follows:

- **Chapter 2** presents the literature review, covering megawatt charging systems, grid code requirements, and challenges related to grid interaction.
- **Chapter 3** describes the system architecture and modeling methodology, including converter design, control strategies, and simulation framework.
- **Chapter 4** presents the results and analysis, including system performance under varying grid conditions and standardized disturbance scenarios such as LVRT, OVRT, voltage variation, and frequency deviation.
- **Chapter 5** provides the conclusions of the study, along with key contributions, limitations, and recommendations for future work.

# 2 Literature Review

This chapter covers the existing literature regarding the megawatt-level charging infrastructure for electric vehicles, concentrating on topics such as architectural design, grid connection issues, and power quality effects. In addition to this, it also looks at the impact of the grid strength and converter structure on system operation. The chapter sets up the groundwork for the analysis in the following chapters.

## 2.1 Overview of Megawatt-Scale Charging Systems

The electrification of the transport system, particularly long-haul cargo transportation and fleets, has become increasingly common, necessitating megawatt charging technology capable of delivering significant amounts of power in a relatively short period of time. In these cases, charging duration directly impacts operational efficiency, and megawatt-class charging infra-structure is essential to enabling electrified freight transportation (Habib et al., 2018).

The design of megawatt chargers is achieved through cascaded stages of the power electronics system, that include the grid-tied AC-to-DC stage and the galvanically isolated DC-to-DC stage. The first stage is charged with the tasks of performing AC-to-DC conversion and controlling the voltage level on the DC-link as well as managing the exchange of energy between the grid and the charger. The second stage is tasked with isolating the power supply and battery charging using CC-CV controls. It is quite common to implement such a two-stage approach due to its advantages of modularity, scalability, and compliance with safety features (Habib et al., 2018; Mohamed et al., 2023; Wang et al., 2012).

Operating at megawatts requires some considerable engineering considerations, which include efficiency of conversion, thermal issues, and electrical stress. Conductive losses

are high in high currents, while losses incurred from switching depend greatly on both topology of the converter and the switching frequency. In this case, a consideration of efficiency vs. cost needs to be made, together with consideration of power quality at PCC (Wang et al., 2012).

Besides design aspects, megawatt chargers also have characteristics similar to that of interactive power electronics rather than passive loads because of their higher power needs and dynamic control systems that could influence grid voltage and produce harmonics owing to their aggregated character (Blaabjerg et al., 2006; Mohamed et al., 2023). The above effect is common with interactive converter-based systems connected to the grid due to the interaction of the control process with system impedance (Blaabjerg et al., 2006).

Grid-side converter performance is crucial to the behavior of the entire system. In power conversion systems, two-level and three-levels are among those frequently used, with each of them having its pros and cons concerning such aspects as efficiency, switching losses, and harmonic performance. Multilevel converters have proven advantageous due to their lower voltage stresses, high-quality waveforms, and minimized harmonics, which make them ideal for MW-level applications (Rodríguez et al., 2002; Texas Instruments, 2021).

In order to comply with the power quality specifications, filters, including LCL filters, need to be used to avoid any harmonic injection into the grid system. Filter efficiency is dependent on its coordination with the converters' control methods and the impedance of the grid system, especially when dealing with high-power systems (IEEE Standards Association, 2020). Although LCL filters exhibit better harmonic suppression, their stability depends heavily on the grid impedance and may need further damping techniques, especially in a weak grid environment (Liserre et al., 2006). However, a simple RL filter is adopted in this study to ensure robust operation across different grid strengths.

While actual systems may consist of many parallel charging stations, the study of individual charging stations is important for obtaining a better understanding of the basic principles and operations involved in converting and connecting to the electrical grid

## 2.2 Battery Sizing Trends and Industrial Perspective for Heavy-Duty EVs

Regarding the electrification of heavy-duty transports, there has been a substantial increase in the demand for energy storage on board in comparison to passenger electric vehicles. The battery size capacity used for passenger electric vehicles is around 50-100kWh while battery sizes used in heavy-duty electric vehicles especially those long-distance truck vehicles and buses are much larger than passenger vehicles' battery sizes (Moorthy et al., 2024). In the literature, it has been reported that HD-EV battery sizes are in the range of 250-750kWh (Moorthy et al., 2024).

Considering the infrastructure aspect of the topic, the emergence of Megawatt Charging System (MCS) technology is directly related to this increasing trend in battery sizes. Ultra-fast charging is essential because of the need for high-capacity batteries since they provide more range in logistics activities and this requires ultra-fast charging. As a result, 700-800 kWh battery sizes have become common in research and industrial applications (Althurthi & Rajashekara, 2025). Significantly, these assumptions have been validated through recent advancements within industry.

As shown in **Figure 2-1**, the Mercedes-Benz eActros 600 model comes with a capacity of about 600+ kWh in batteries (Mercedes-Benz Trucks, 2024), whereas the Volvo FH Aero Electric variant is estimated to possess up to ~780 kWh battery capacity when configured as an extended-range version (Volvo Trucks, 2024). Also, Scania Electric Truck series features modular batteries that can exceed 700+ kWh (Scania Group, 2024), and the Tesla Semi is expected to have a capacity of 800+ kWh (Tesla Inc., 2023). Therefore, batteries in the order of 600-800+ kWh capacity are currently being utilized and are even being aimed for commercial trucking operations. Considering all these insights, we have considered designing a battery of size approximately 750 kWh in this study.

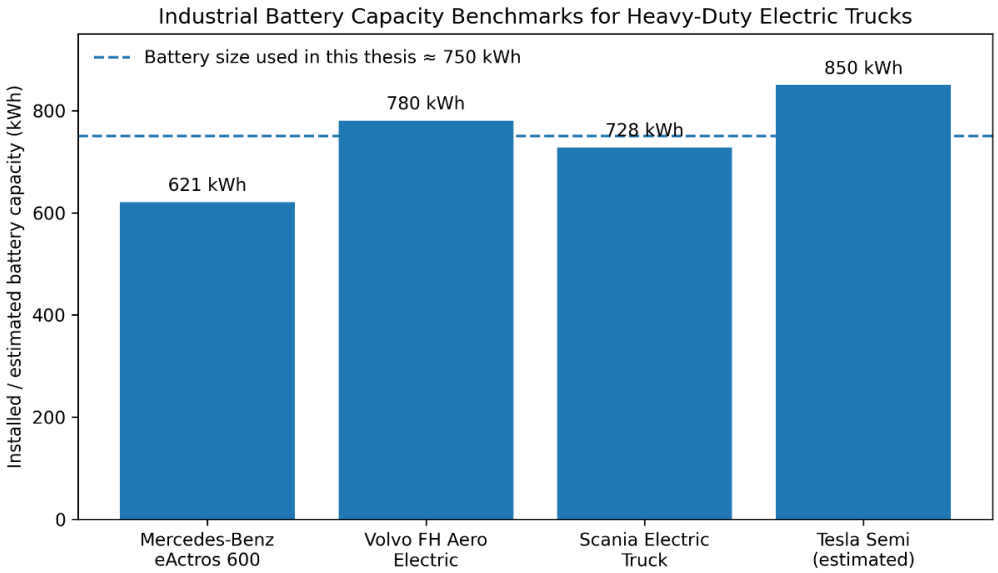


**Figure 2-1:** Industrial battery capacity benchmarks for selected heavy-duty electric trucks, Source: Developed using Python by Author

Thus, using batteries of such large capacities is justified based on both the requirements from literature sources and industrial practice. This means that the use of batteries with high capacities can be employed in simulations focused on studying megawatts-level charging capabilities of battery-powered trucks and their impact on the electricity supply network.

## 2.3 Grid Integration Challenges of High-Power EV Charging Systems

The incorporation of EV charging systems in electrical distribution systems at the megawatt scale presents major problems for power quality, voltage stability, and dynamic effects. Unlike traditional electrical loads, EV chargers use mainly power converters. Due to fast switching and the closed-loop control dynamic response of power converters, interaction effects might take place between the power converter and the grid impedance (Habib et al., 2018; Blaabjerg et al., 2006).

Measurement-based studies and simulation-based study indicate that harmonic distortion levels in EV charging systems vary considerably with changes in operating conditions

and network characteristics. This variability underscores the necessity of system-level analysis (Nikitha et al., 2017).

Voltage stability at the PCC must not be neglected. Charging systems with high power may cause problems with voltage drop and flicker, particularly in the distribution network, which has low short-circuit capacity. Power grid stability is assessed using short circuit ratio (SCR). Low SCR denotes poor grid stability and more risks when it comes to high-power charging.

In the case of weak grids, the interaction of the converter control system and the grid impedance plays an important role. In particular, lower SCR values lead to increased coupling and cause the system to behave with poor stability margin and poorer control performance (Huang et al., 2021). This effect is even magnified by megawatt-class chargers.

Grid synchronization also poses an additional problem to deal with. Grid synchronization usually employs the phase-locked loop (PLL), but PLL performance can suffer when the grid becomes weak or distorted; some research works suggest that such situations might lead to grid instability and harmonics injection into the grid system. Topology and control choice for the converter may have a great influence on grid synchronization too (Blaabjerg et al., 2006; Huang et al., 2021; Texas Instruments, 2021).

According to the literature, the ability of the system to tolerate disturbances like dips, swells, and frequency variations on the network is critical. The fault ride-through capability is crucial, and for this, proper planning is necessary concerning the converters and protection systems (ENTSO-E, 2023).

Multiple high-power chargers may cause aggregated impacts to the grid when deployed in specific zones like depots and highway stations. Such impacts may involve heavier loads on feeders, higher stress on transformers, and network congestion. Even though

this research focuses on one charger, studying how it works in the context of the grid provides a basis for analyzing larger systems (Habib et al., 2018).

To sum up, the integration of megawatt-scale electric vehicle charging systems needs an overall perspective for taking into account the converter, the controller, and the electric power grid at once. Such an overall perspective is vital to ensure stable operation under steady-state and dynamic conditions.

## 2.4 Weak Grid Characteristics and SCR-Based Classification

The relationship between grid-connected power electronic devices and the electric grid depends heavily on grid strength, which can be quantified by the short-circuit ratio (SCR). This parameter is calculated based on the short circuit apparent power available at the point of common coupling (PCC) relative to the power rating of the converter, giving a measure of the grid's capability to sustain voltage stability under load changes.

Generally, the higher the SCR value, the stronger the system and more uniform its voltage profile; on the other hand, the lower the SCR, the weaker the system and more sensitive it becomes to external factors. It shows high impedance and strong coupling with the grid. Typically, classifications indicate that systems with SCR values of 6-10 are considered weak, while those with SCR values greater than 20 are considered robust (Huang et al., 2021), but these classification criteria mostly apply to transmission systems.

For megawatt-scale charging systems, a more stringent classification is required to reflect practical operating conditions. In this study, the following SCR-based categorization is adopted:

- **Weak grid: SCR ≤ 3**
- **Moderate grid: 3 < SCR ≤ 12**
- **Strong grid: SCR > 12**

This stricter classification accounts for the increased sensitivity of high-power converters to grid impedance, even at moderate SCR values.

For a weak power grid, the relationship between the controller of the converter and the grid impedance becomes significant. The higher the grid impedance, the more tightly coupled the system becomes. This can cause oscillation, decreased damping, and instability. All of these factors are accentuated due to the fast dynamic behavior of megawatt chargers.

Grid synchronization becomes especially vulnerable in weak grids. The PLL used for estimation of the phase and frequency of the grid voltage can perform poorly due to distortion or weakness, causing system to become unstable and inject more harmonics (Huang et al., 2021). Apart from stability issues, another characteristic of poorly constructed grids is poor power quality, which includes increased THD and voltage ripples at the point of common coupling (PCC). This is caused by the limited short circuit capacity, which makes it difficult for the grid to tolerate harmonics.

However, when the grids are robust, they offer stability for operations due to lower impedance levels, smaller fluctuations in voltage, and less interactions between the converters and grid system. Furthermore, in this situation, it is the characteristics of the converters that determine the operation of the system, instead of the grid limitations. The grid impedance, in this case, is modeled as an R-L equivalent, referred to the point of common coupling at 690 V. The X/R ratio used was 10 to represent an inductive industrial distribution supply, normally associated with an upstream MV grid and transformer connection.

In conclusion, the strength of the grid plays a very important role in the study of megawatt-scale EV chargers in terms of stability and power quality. It is vital to test the operation of such systems at various SCR values in order to assess their performance accurately.

## 2.5 Grid Impact and Power Quality in Megawatt EV Charging System

The adoption of megawatt scale charging systems for electric heavy-duty vehicles poses considerable problems to the power system because of their substantial power requirements, high loading density, and use of power electronics for grid interface (Nikitha et al., 2017). It also provides some opportunities including improved power management and grid support , hence we can say that it plays a dual role by affecting power quality while also enabling operational flexibility as shown in **Figure 2-2** (Das et al., 2020). In terms of systems, the transition from fuel-powered to electric heavy-duty transportation does not imply any major increase in energy use; nevertheless, the impact on power usage patterns will be significant, especially in terms of peak demands and localized grid load impacts (ENTSO-E, 2023). It is apparent that the problem with integrating such systems into the electricity grid does not lie in the energy supply capacity.

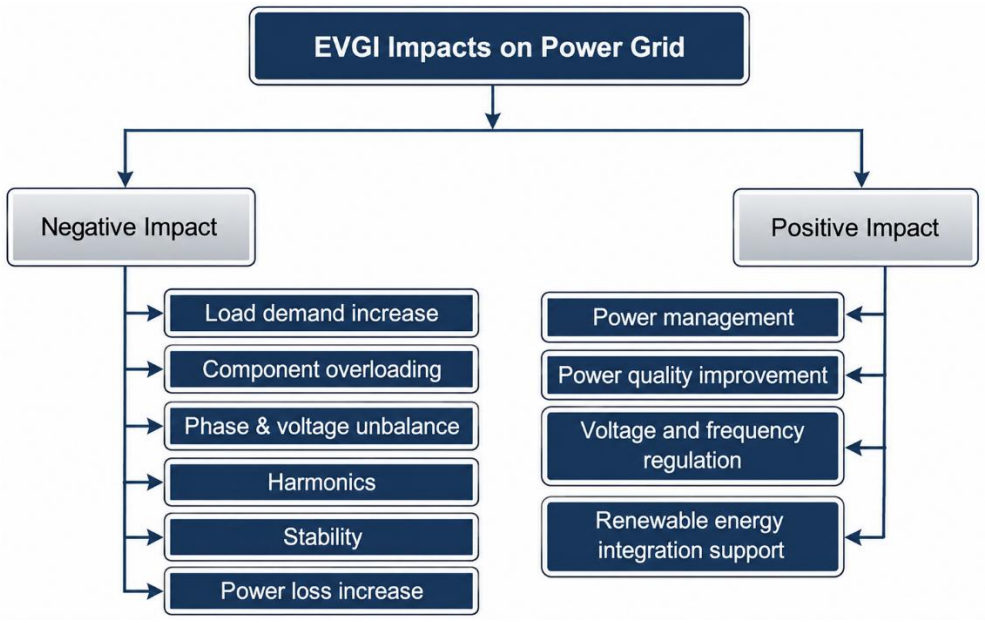


**Figure 2-2** : Impacts of EV Grid Integration, Source: Adapted from Das et al. (2020).

Charging infrastructure is typically deployed in clusters at depots or logistics hubs, where multiple vehicles charge simultaneously over short durations. This results in sharp demand peaks, voltage fluctuations, and increased stress on network components,

requiring careful planning and coordinated operation (ENTSO-E, 2023). In addition to demand-related challenges, megawatt-scale charging systems introduce power quality concerns due to their reliance on high-power electronic converters. Active front-end converters regulate power exchange with the grid but also inject harmonic currents due to high-frequency switching, with the resulting distortion strongly influenced by grid impedance. It has been proven that harmonic distortions and voltage variations are considerably magnified in weak grids, where the low short circuit strength of the grid decreases its capacity to withstand perturbations (Zhu et al., 2020). Thus, similar converter configurations can generate increased voltage total harmonic distortion (THD), and this should be analyzed in line with the existing power quality criteria (IEEE Standards Association, 2020; Zhu et al., 2020).

It is even more important in medium voltage distribution grids, where high power charging results in significant voltage drops in the network, which then spread throughout the whole network. This phenomenon of voltage drop becomes even more pronounced when several chargers operate simultaneously. Moreover, high peak loads, together with harmonic loads, cause higher RMS loading of transformers and feeders, leading to faster deterioration and shorter lifetimes for equipment (Zhu et al., 2020). Thus, issues related to power quality go beyond problems of waveform distortions. These problems aside, megawatt-scale charging systems have their own advantages in terms of supporting the power grid as well. This is made possible through their controllability, which can be used to implement peak shaving, load shifting, and better integration of renewable energy, among other measures (ENTSO-E, 2023).

In this thesis, the power quality in terms of critical parameters like harmonic distortion, DC-link voltage ripples, and battery-side ripples is examined at the converter level. The examination of power quality characteristics under various levels of grid.

## 2.6 Converter Topologies for Megawatt- Scale EV Charging System

Selecting the right topology is vital to ensure high efficiency, proper power quality, and grid stability during the charging of electric vehicles on a megawatt level. With the increase in the level of power, certain limitations can be seen in the traditional topology of the converters, making the choice of topology an essential factor in the design of these systems. High power charging stations generally operate with a voltage source converter-based active front-end (AFE), providing the ability to regulate the DC link and comply with the grid regulations. The overall performance of this stage is influenced by converter topology, switching strategy, and filter design (Blaabjerg et al., 2006).

### 2.6.1 Two Level Converter Topology

Two-level (2L) inverters have found wide application because of their simplicity, reliability, and easy control. Two different voltage levels are produced per phase of the inverter, enabling easy modulation and realization. Nevertheless, when high powers are involved, some problems start emerging such as high switching losses, high voltage stresses on semiconductors, and increased harmonic distortion. Consequently, larger filter demands may arise for good power quality (Texas Instruments, 2021).

### 2.6.2 Three-Level Converter Topology

The use of 3-level converters, which include the NPC structure, is typical in medium to high power applications due to their ability to produce more voltage levels that minimize voltage transition steps, thereby providing better waveforms and less switching stress. The latter leads to lesser harmonics and increased efficiency; hence, multilevel converters are preferable for megawatt systems because of the above qualities. Nevertheless, there is a downside associated with these converters – namely, higher complexity of control and hardware costs (Rodríguez et al., 2002). In three-level NPC converter, a neutral point balancing controller was proposed for keeping the DC-link capacitor voltages balanced and minimizing distortion and switching losses (Celanovic & Boroyevich, 2000).

### 2.6.3 Topology and Grid Interaction

Converter topology selection is directly related to how well it interacts with the grid, especially regarding harmonics and stability. When the grid conditions become weak and have a very low short-circuit ratio (SCR), there will be a critical sensitivity of the grid impedance to the converter's control mechanism. Studies on inverter-based grid interactions show that control scheme and converter topology greatly affect stability and harmonics (Huang et al., 2021).

### 2.6.4 Motivation for Comparative Evaluation

With all these tradeoffs existing between the converter topology and its dependency on the grid environment, there is no doubt that a comparative study is needed to determine their compatibility in megawatt scale charging stations for electric vehicles. This is what this thesis aims to do by examining various converter topologies and how they react to different grid environments.

## 2.7 Standards and Grid -Code Framework for Megawatt Charging Systems

The assessment of high-power charging stations should take into account the standards of EV charging equipment as well as the standards on grid integration. In this study, the standard IEC 61851-23-3 will serve as the principal standard to assess DC chargers, while the standard EN 50549-2 is considered the key standard for grid interaction.

The IEC 61851 series comprises a set of standards for conductive charging, and specifically the IEC 61851-23 standard establishes the requirements for the EVSE chargers of the DC type, thus laying the foundation for the secure energy transfer between the power grid and the electric vehicles. Further development into MW chargers is proposed in IEC 61851-23-3, which is currently under development and establishes the standards for the Megawatt Charging System (MCS), where the supply side voltage (Side A) would comprise up to 1000 V AC or 1500 V DC, whereas the voltage on the vehicle side (Side B)

would comprise up to 1250 V DC (IEC, 2024). Nevertheless, certain features are still being discussed, for example, higher voltages, bidirectional operation (V2G), or other system architectures. This implies that megawatt chargers develop faster than the relevant standardization, and hence such standards should be viewed merely as preliminary recommendations. This is why the present paper uses standards as references for the analysis and evaluation according to the characteristics of their converters and interaction with the grid network.

Although IEC 61851 deals with EV charging functionalities, it does not cover the behavior of converters during grid disturbances. For this matter, EN 50549-2 contains pertinent information related to systems that are grid-connected in medium-voltage grids, considering their operations during abnormal voltages and frequencies (CENELEC, 2019). Even though EV charging systems do not fall into the category of generator systems, the grid-side Active Front End (AFE) shares common features with conversion generator systems. In this regard, EN 50549-2 will be utilized as the basis for assessing the system's behavior during disturbances like LVRT, OVRT, steady state voltage variation (+/- 10%), and off nominal frequency operation.

Other specifications such as IEC TS 63379 that apply to the charger interface, ISO 15118 for the communication process, and EN 50160 for voltage quality have been mentioned; nonetheless, these standards are not applicable to the scope of this study, which will concentrate only on the technical side of power flow and integration into the grid. Harmonic assessment has been performed based on current distortion limits (THDi) according to IEEE 519 (IEEE Standards Association, 2020) and not voltage distortion as defined in EN 50160, due to the fact that voltage distortion depends on the characteristics of the source upstream of the charging station.

On that reference, this thesis will utilize an assessment methodology based on simulations called Grid-Integrated MCS Validation Framework (GMVF). In this case, IEC 61851-23 establishes the foundation for EVSE functionality, IEC 61851-23-3 is used as the newly

introduced MCS reference standard, EN 50549-2 is applied to define the criteria for disturbance assessment, while IEEE 519 will be used to address issues related to harmonic current distortion.

## 2.8 Grid-Integrated MCS Validation Framework (GMVF)

The previous parts have discussed significant concerns related to megawatt-scale charging stations, such as grid strength considerations, dependence on converter technology, and developing standards. In this regard, an evaluation methodology should be considered to evaluate the performance of such systems in real-world grid scenarios.

In this study, the Grid-Integrated MCS Validation Framework (GMVF) technique is selected as the main approach to assess the results of the research. Grid codes are not regarded as mandatory compliance standards here; rather, GMVF facilitates systematic analysis of converter performance under various disturbances obtained from the grid code regulations, providing a practical framework for analyzing grid compatibility during the design and development phase.

The key benefit of the GMVF system is the transformation of standard operation parameters to simulated tests, where the behavior of the system can be studied in depth without requiring physical validation. This is especially useful when considering megawatt scale charging systems due to limited testing facilities and cost. The disturbances in this study have been taken from EN 50549-2 and include voltage dips & swells with recovery, steady-state variations in the voltage (±10%), and frequency deviations.

Though these are not meant for showing formal compliance to the standards, they present realistic stress conditions that the system can be tested on to assess its stability (Moorthy et al., 2024). GMVF considers system response over theory, which means that performance will be based on factors like harmonic distortion, dc link voltage characteristics, and ripples on the battery side. The use of these parameters ensures a consistent

basis for measuring system performance when compared to varying grid strength and converters.

One of the important contributions made by this dissertation is the implementation of GMVF in a variety of grid cases, such as weak grids, moderately strong grids, and strongly stable grids. This enables us to set the limit of system performance and gain information regarding when the system starts performing poorly.

In summary, besides being a compliance-driven analysis tool, GMVF is equally applicable as a design tool, thus enabling evaluation of converter topologies in real-world operating environments. GMVF constitutes the basis of the methodology underlying the simulations and analyses carried out in the chapters that follow.

# 3 Methodology and System Modeling

This chapter discusses the approach that was followed for analyzing the megawatt-level charging system. This includes discussing the architecture of the system, the assumptions behind designing the system, and the control methods applied. The chapter lays down the groundwork for conducting simulations described later in other chapters.

## 3.1 Methodology Overview

This study adopts a simulation-based methodology to evaluate the performance of a megawatt-scale electric vehicle charging system under realistic operating conditions. The approach, referred to as Grid-Integrated MCS Validation Framework (GMVF), integrates system modeling, control design, and structured performance evaluation within a unified framework. The key parameters of the grid, converter, and battery system used in the simulation model are summarized in **Appendix A — System Parameters.**

The methodology is designed to capture both electrical behavior and grid interaction of high-power charging systems without reliance on physical prototypes. The simulation is performed using an EMT-based modeling approach, and the corresponding solver configuration is provided in **A.9 Simulation Solver Configuration** The overall approach consists of the following steps:

- Development of a detailed system model that includes the grid interface, active front-end (AFE), DC–DC converter, and battery representation.
- Implementation of control strategies for grid-side power regulation and battery charging, utilizing a grid-following architecture and constant current–constant voltage (CC–CV) control.
- Integration of protection and supervision mechanisms in accordance with IEC 61851-23-3 requirements.
- Definition of performance metrics for power quality, voltage stability, and battery-side stress.

- Simulation of the system under both steady-state and disturbance conditions, including grid voltage variations and ride-through scenarios.
- Post-processing of simulation signals to extract harmonic distortion, voltage ripple, and battery current ripple aligned with IEC standards.

This structured methodology enables consistent and repeatable evaluation of system performance across various operating conditions. It also provides a practical framework for assessing grid-code-relevant behavior of megawatt charging systems, while maintaining alignment with emerging standards and realistic converter dynamics.

## 3.2 System Overview

This project develops a megawatt-class electric vehicle charging system (MCS) model to assess converter performance, grid interaction, and compliance under real-world conditions. The model uses MATLAB/Simulink and simulates a single high-power charging unit at 690 V AC, 50 Hz, supplying power to a high-voltage battery through a multi-stage conversion architecture.

The selected topology, shown in **Figure 3-1**, consists of:

- A grid-connected active front-end (AFE) for controlled AC–DC conversion
- A DC-link (~1200 V) acting as an energy buffer
- An isolated DC-DC stage for voltage adaptation and battery charging

This architecture reflects practical MW charging systems, where grid-side controllability, electrical isolation, and battery-side regulation are decoupled to ensure stable and scalable operation.

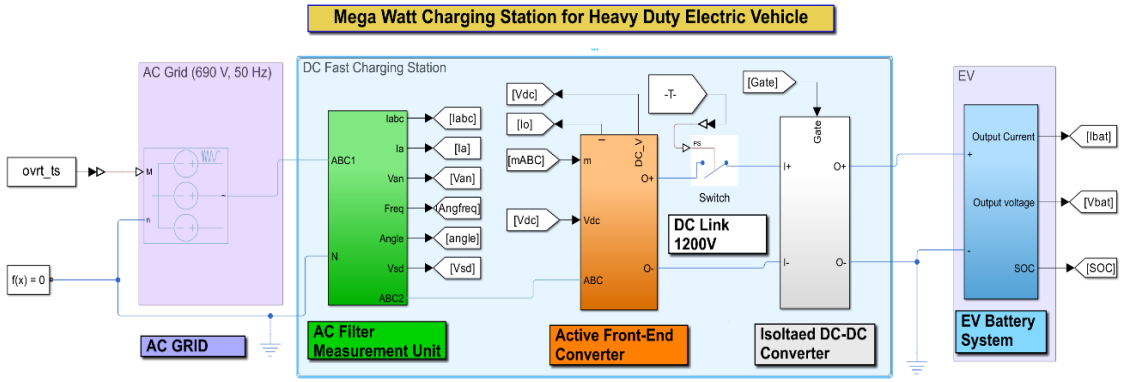


**Figure 3-1**: System-Level Architecture of the Megawatt Charging System

Above **Figure 3-1** is a simplified representation of the megawatt charging system implemented in Simulink, illustrating power flow from the 690 V AC grid through the active front-end (AFE), DC link (~1200 V), isolated DC–DC converter, and to battery system. Internal control and measurement signals are retained for completeness but are not central to system-level interpretation.

The system is built to work in the 1.2 to 1.5 MW range, using high DC-link voltage and controlled current flow. This power level suits heavy-duty charging and is used to study grid impact and control performance in different situations.

## 3.3 Modeling Approach

This chapter describes the modeling approach and system architecture utilized in the megawatt-scale charging system. The models, controls, and protections applied for the purpose of system simulation and analysis are also explained. This chapter also outlines the methods for performance assessment and power quality analysis.

### 3.3.1 Modeling Philosophy

The model is developed using a control-oriented, system-level approach, where the objective is to capture:

- Converter control dynamics

- Power quality at the grid interface
- Interaction between subsystems under disturbances

Rather than detailed semiconductor-level modeling, the focus is placed on electrical behavior and control response, which are the dominant factors influencing grid compliance and system performance.

This approach ensures that the model remains computationally efficient, while retaining sufficient fidelity for evaluating LVRT/OVRT response, harmonic behavior, and charging dynamics.

### 3.3.2 Standards-Aligned Modeling (IEC61851-23-3)

The system's architecture and operating conditions comply with IEC 61851-23-3, the standard that establishes the standard operating procedure for megawatt charging systems.

This standard serves as the main reference for modeling decisions, especially in these areas as follows:

**Voltage Levels and System Scaling**

- The DC-link voltage, about 1200 V, and the battery interface are chosen to fit within the range set for megawatt charging systems. On the vehicle side, this goes up to about 1250 V DC, with even higher levels being considered.
- The 690 V AC interface is a practical industrial supply level that feeds high-power chargers through an upstream transformer.

**Energy Transfer Architecture**

- The separation between grid-side (AFE) and vehicle-side (DC–DC) conversion reflects the standard's definition of distinct supply and EV domains.
- Adding an isolation transformer in the DC–DC stage meets safety and functional requirements for galvanic isolation.

**Controlled DC Link Switching**

This switch acts as a control interlock for starting purposes between the DC link and the isolated DC-DC section as shown in **Figure 3-1** . This switch stays open while starting the

converter system to enable the stabilization of the DC bus and then is closed after around 80 milliseconds once safe operating condition is verified by the protection supervisor.

**Operational Characteristics**

- The system is modeled as unidirectional, which matches current implementations. Bidirectional (V2G) requirements are still being developed in IEC61851-23-3 standard.
- Controlled energy transfer is achieved by coordinating converter operation instead of using passive rectification.

**Protection and Monitoring Philosophy**

- Although detailed protection logic is not included, the model monitors DC-link voltage, battery terminal voltage, and current. This reflects the standard's focus on safe and controlled operation.
- Architecture naturally supports isolation and controlled energy flow, both of which are key to MCS design.

IEC 61851-23-3 sets system-level requirements but does not specify detailed converter control strategies. So, while the architecture and operating conditions follow the standard, the control implementation (PLL design, current regulation strategies) and performance evaluation are developed specifically for this study.

### 3.3.3 Grid Representation and Interface

The grid is modeled as a Thevenin equivalent with a series RL impedance. This setup allows the grid strength to be adjusted using the short-circuit ratio (SCR), so it can simulate strong, moderate, or weak grid conditions. This approach makes it easier to study how the converter and grid interact under different network stiffness levels**. Figure 3-2** illustrates the grid interface as follows :

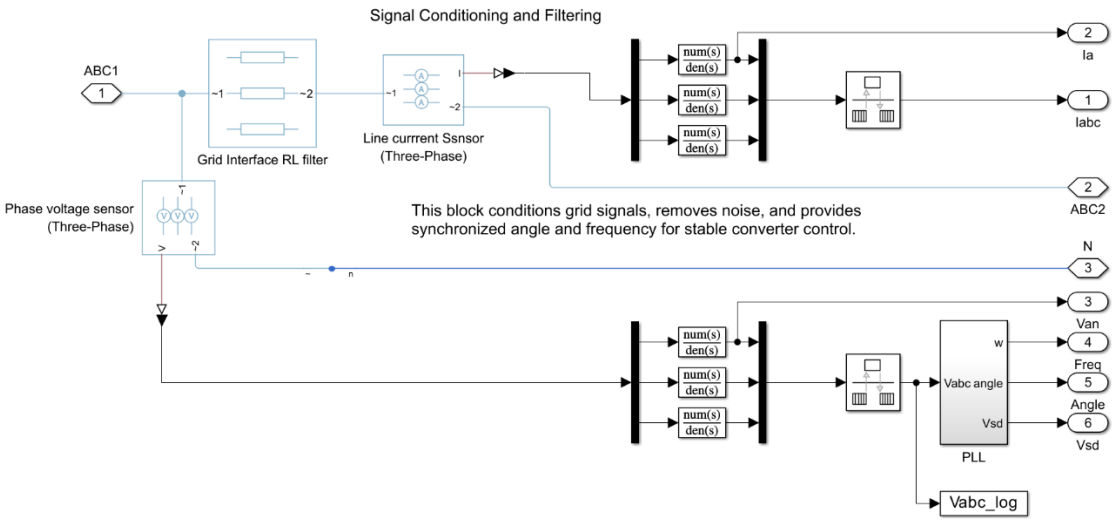


**Figure 3-2**: Grid Interface, Measurement, and Synchronization for AFE Control

The RL-based grid interface incorporates three-phase voltage and current measurement. Signal conditioning is applied to provide stable inputs for synchronization and control. A phase-locked loop (PLL) is used to extract the grid angle and frequency, enabling precise converter synchronization.

The RL filter accurately represents grid impedance and serves several important purposes:

- It limits current ripple at the point of common coupling.
- It attenuates high-frequency harmonic components.
- It establishes a controlled electrical interface between the converter and the grid.

Three-phase voltage and current signals are measured and then processed through signal conditioning blocks to keep the data stable and reduce noise. These conditioned signals go to a phase-locked loop (PLL), which estimates the grid angle and frequency needed to synchronize the active front-end converter.

This setup provides reliable synchronization and stable converter operation under different grid conditions, even when the grid is weak and its impedance has a big impact on system behavior.

### 3.3.4 Active Front-End Converter

The grid-connected interface of the charging system is realized using a three-level neutral-point clamped (NPC) active front-end (AFE) converter. This topology is selected to enable high-power operation with improved efficiency, reduced harmonic distortion, and lower voltage stress on semiconductor devices compared to conventional two-level converters. Refer **Appendix A — System Parameters** Table A.2 for more parameters in detail.

The AFE structure is shown in **Figure 3-3** is a converter interfaced with a split DC-link formed by two capacitors, which divide the total DC voltage into two levels. This configuration enables the generation of three discrete voltage levels at the converter output, resulting in reduced dv/dt stress and improved current waveform quality at the grid interface. A detailed calculation of the DC-link energy buffering capability is presented in **A.8 DC Link Energy Buffering Time.**

**The split DC-link performs several critical functions:**

- Provides short term energy buffering between the AC and DC stages
- Enables voltage sharing/balancing across semiconductor devices
- Supports multilevel voltage synthesis for improved power quality

Voltage balancing across the DC-link capacitors is maintained through appropriate modulation and control strategies, ensuring stable converter operation under varying load and grid conditions. This is particularly important in three-level topologies, where imbalance in capacitor voltages can affect switching performance and overall system stability. In addition, DC-link voltage and current measurements are incorporated to support converter control and system monitoring. These measurements are essential for maintaining DC voltage regulation, ensuring controlled power transfer, and enabling coordination with the downstream DC–DC conversion stage.

The use of a three-level NPC AFE is particularly advantageous in megawatt-scale charging systems, where efficiency, power quality, and device reliability are critical design considerations, especially under weak grid conditions.

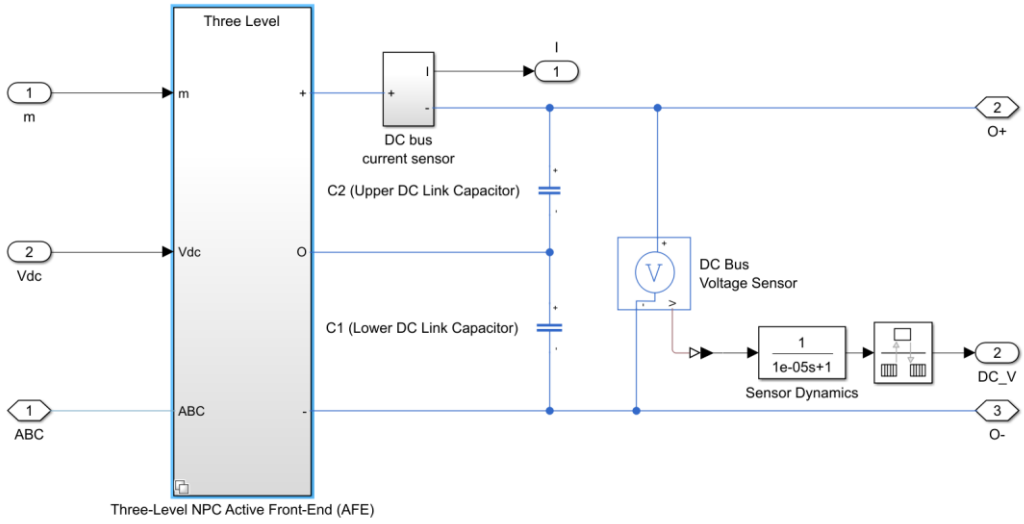


**Figure 3-3**: Three-Level NPC Active Front-End Converter and DC-Link Structure

Representation of the active front-end (AFE) converter based on a three-level neutral-point clamped (NPC) topology. DC-link voltage and current measurements are included for control and monitoring purposes.

In addition to the three-level NPC topology, a conventional two-level (2L) voltage source converter is also implemented within the same simulation framework for comparative analysis. The two-level configuration follows the same control structure and operating principles but utilizes a simpler switching scheme with higher voltage stress and reduced harmonic performance. This allows a consistent evaluation of the impact of converter topology on power quality, DC-link behavior, and grid interaction under identical operating conditions.

The switching frequency of the active front-end converter is set to 10 kHz, providing a practical balance between current control bandwidth and switching losses at megawatt-

scale operation. This selection ensures effective harmonic mitigation while maintaining stable DC-link regulation under varying grid conditions.

### 3.3.5 Active Front-End Control Strategy

The active front-end (AFE) converter is controlled using a grid-following vector control scheme, as illustrated in **Figure 3-4**.

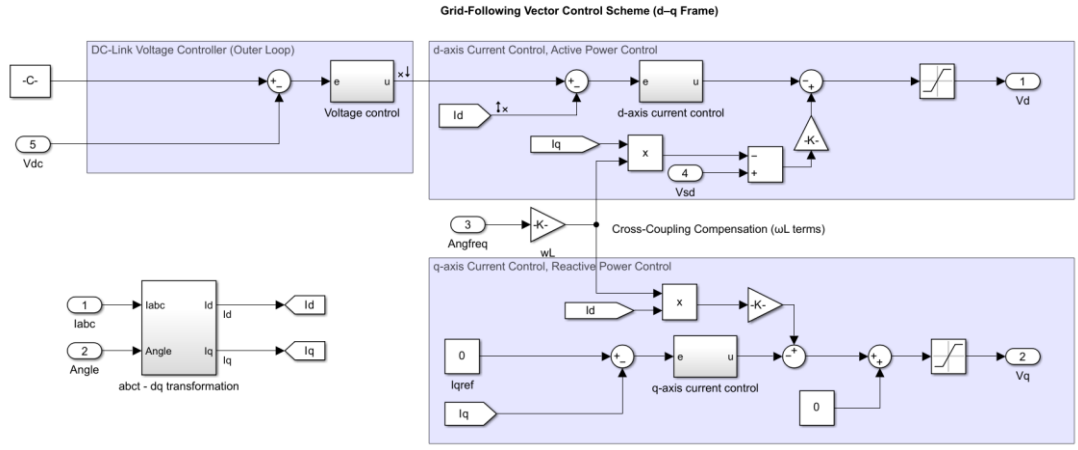


**Figure 3-4**: Grid-Following Vector Control Scheme of the Active Front-End Converter

d–q reference frame control structure consisting of an outer DC-link voltage control loop and inner current control loops. Cross-coupling compensation and feedforward elements are included to enhance dynamic performance and stability during grid-connected operation.

The control architecture is based on synchronous reference frame transformation, where grid currents are regulated in the d–q domain. The control strategy is defined as follows:

- A phase-locked loop (PLL) provides grid angle information for synchronization.
- The d-axis current component is used to regulate active power and maintain the DC-link voltage.
- The q-axis current component is set to zero to ensure unity power factor operation.

An outer voltage control loop generates the reference for the d-axis current, ensuring stable DC-link voltage regulation. Inner current control loops regulate the d- and q-axis currents, providing fast dynamic response and accurate current tracking.

To improve dynamic performance and stability, decoupling terms are included to compensate for cross-coupling effects between the d- and q-axes. In addition, feedforward components are incorporated to enhance disturbance rejection and transient response. The selection of a grid-following control strategy is intentional, as it provides:

- Predictable current injection into the grid
- Stable operation under grid disturbances
- Compatibility with grid-code-based evaluation frameworks such as EN 50549-2
- Widely practiced in current E-mobility industrial level applications.

### 3.3.6 DC-DC Converter Modeling

The battery interface is realized using an isolated DC–DC converter, as shown in **Figure 3-5**. This stage is responsible for transferring power from the DC-link to the battery while ensuring electrical isolation and appropriate voltage matching. Refer **A.4 DC–DC Converter** for more information about the parameters associated to it.

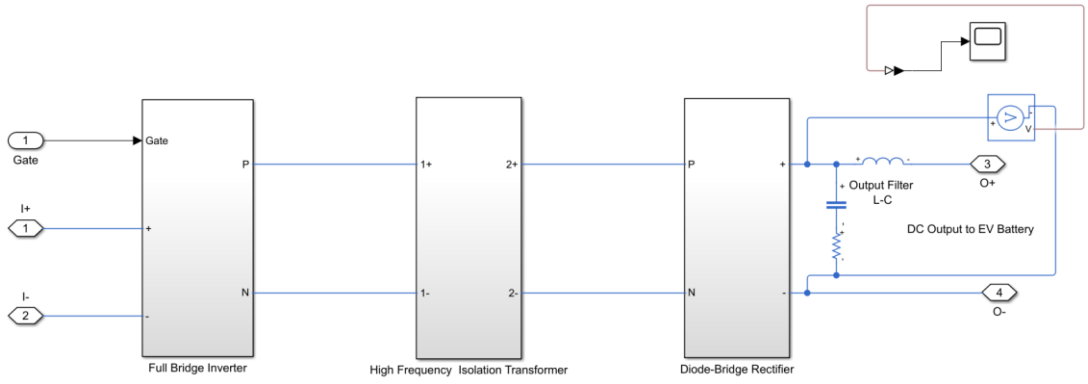


**Figure 3-5**: Isolated DC–DC Converter Topology for Battery Charging

It mainly consists of full-bridge inverter, high-frequency isolation transformer (40kHz), diode-bridge rectifier, and output filter form the battery-side conversion stage.

The converter operates by converting the DC-link voltage into high-frequency AC using a full-bridge inverter. This high-frequency signal is transferred through an isolation transformer, which provides galvanic isolation and enables voltage adaptation. On the secondary side, the transformer output is rectified using a diode-bridge rectifier and filtered to produce a stable DC output suitable for battery charging.

**The DC–DC converter provides the following key functions:**

- Galvanic isolation between the grid-connected stage and the battery
- Voltage adaptation through transformer turns ratio.
- High-frequency power transfer enabling compact design

The output filter reduces switching ripples and ensures smooth current delivery to the battery, which is critical for maintaining battery lifetime and compliance with charging standards.

The use of a diode-bridge rectifier results in inherently unidirectional power flow, restricting operation to charging mode. This design choice simplifies control and aligns with current megawatt charging system implementations, where bidirectional operation is not yet widely standardized.

The design of the battery-side output filter is constrained by requirements defined in IEC 61851-23-3. In particular, the standard specifies that the side B inductance of the EV supply equipment shall be limited to values below 100 µH (IEC, 2024). This limitation is imposed to ensure safe operation during abnormal conditions such as short-circuit and load-dump scenarios, where excessive inductance can result in high stored energy and delayed current decay.

As a result, the inductance value in the present model is selected within this limit, ensuring compliance with protection requirements while still contributing to ripple attenuation. This constraint introduces a practical design trade-off, as increasing inductance reduces current ripple but is restricted by safety considerations defined in the standard.

### 3.3.7 Battery Modeling and Electrical Representation

The battery pack is modeled using a series–parallel configuration of 278 cells in series and 266 parallel strings. Each cell is characterized by a nominal voltage of 3.6 V and a capacity of approximately 2.735 Ah. This configuration results in a pack nominal voltage of ~1 kV and an energy capacity of approximately 748 kWh, consistent with heavy-duty electric vehicle applications, where the terminal voltage is expressed in equation (3.1) as a function of state of charge (SOC) and charging current:

$$V_{\text{term}} = \text{OCV(SOC)} + I \cdot R_0(SOC), \tag{3.1}$$

where OCV(SOC) represents the open-circuit voltage as a function of SOC, and $R_0(SOC)$ denotes the SOC-dependent internal resistance of the battery. The SOC dependent characteristics of OCV and internal resistance used in the model for chosen lithium cell are shown in **Figure 3-6.**

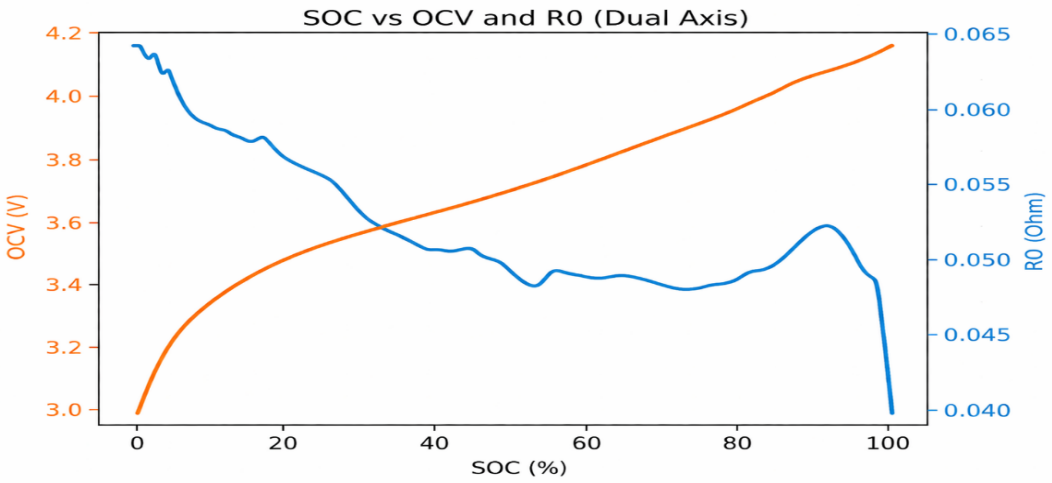

**Figure 3-6:** SOC-Dependent Open-Circuit Voltage and Internal Resistance

The battery model computes the terminal voltage based on the instantaneous charging current and internal resistance, while SOC dynamics are obtained through current integration. This approach captures the dominant electrical behavior of the battery under high-power charging conditions while maintaining computational efficiency. The implemented model structure is shown in **Figure 3-7**.

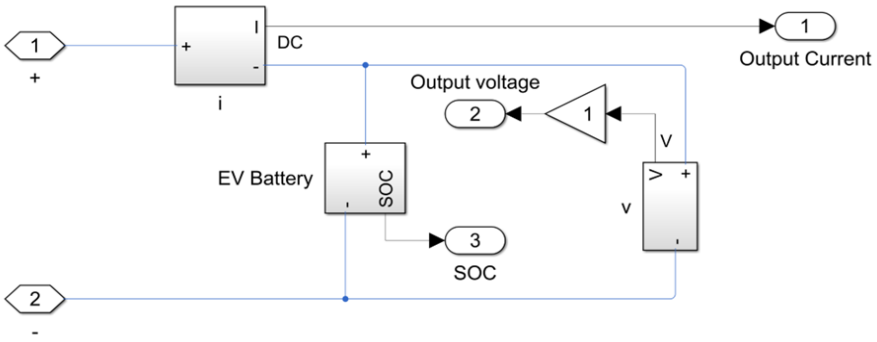


**Figure 3-7**: Battery Model Based on Terminal Voltage Representation

Above **Figure 3-7** is an equivalent electrical model computing terminal voltage and SOC dynamics based on current input and SOC-dependent parameters.

### 3.3.8 Terminal Voltage -Based Control Justification

The distinction between open-circuit voltage and terminal voltage is critical for accurate control of battery charging. Open-circuit voltage represents the equilibrium voltage of the battery in the absence of current flow, whereas terminal voltage reflects the actual voltage under operating conditions.

During charging, the terminal voltage deviates from the open-circuit voltage due to the voltage drop across the internal resistance, as illustrated in **Figure 3-8**. This deviation between terminal voltage and open-circuit voltage caused by internal resistance and charging current.

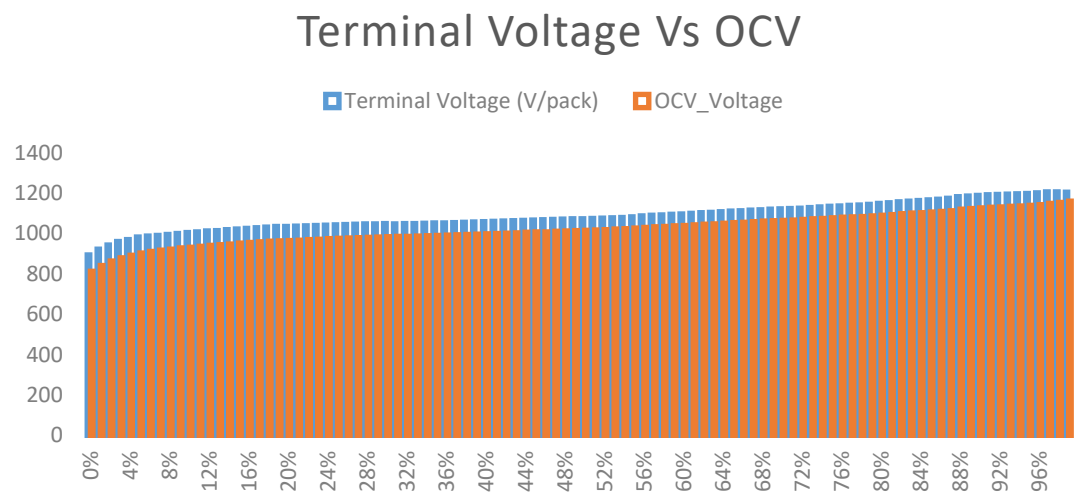


**Figure 3-8:** Terminal Voltage vs Open-Circuit Voltage Under Charging

At megawatt-scale charging levels, the charging current is sufficiently high that the voltage drop across the internal resistance becomes significant. As a result, relying solely on OCV for control would lead to inaccurate voltage regulation and premature transition into constant-voltage operation. Therefore, terminal voltage is selected as the control variable in the charging strategy. This ensures that the control system responds to the actual electrical state of the battery underload, enabling accurate regulation of the charging process and improving overall system reliability.

## 3.4 Charging and Protection Control Architecture

The charging system is governed by a hierarchical control architecture that integrates charging control, protection logic, and DC–DC converter control, as shown in **Figure 3-9**. Basically, it's a supervisory control structure combining CC–CV charging logic, protection mechanisms, and DC–DC converter control.

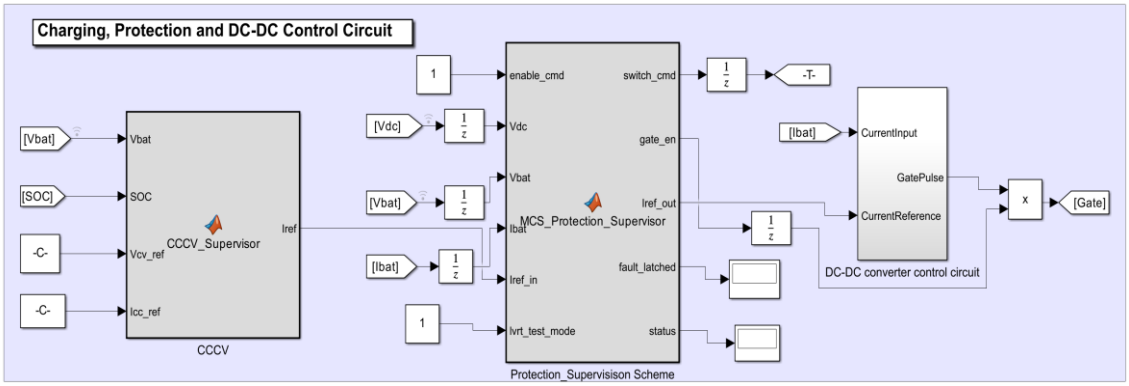


**Figure 3-9**: Integrated Charging, Protection, and DC–DC Control Architecture

We will see more about the functioning of each of these blocks in the following subsections as we progress through, the control architecture consists of three primary layers as follows from subsections 3.4.1 to 3.4.3**:**

### 3.4.1 CC–CV Charging Supervisor

The charging process is managed using a constant current–constant voltage (CC–CV) strategy implemented in the supervisory controller. The controller generates a current reference based on battery terminal voltage and state of charge.

- In constant current (CC) mode, the current reference is maintained at a predefined level to enable fast charging
- In constant voltage (CV) mode, the terminal voltage is regulated while the current reference is gradually reduced

The transition between CC and CV modes is based on combined conditions involving terminal voltage and SOC, ensuring stable and realistic charging behavior for enhanced reliability.

#### 3.4.1.1 Implementation Details of CC-CV Supervisor

The CC–CV supervisory logic is designed with dual-condition transitions and smoothing mechanisms to maintain reliable performance during high-power charging, refer **Appendix F — CC-CV Full algoritm** to get a very detailed view of applied logic. The transition

from constant current to constant voltage mode is activated only when both the terminal voltage and state of charge surpass preset thresholds as shown in **Figure 3-10**: CC to CV Transition. By requiring both conditions to be met, the system avoids premature transitions caused by brief voltage fluctuations. To prevent switching back and forth between CC and CV modes, hysteresis is added to both the voltage and SOC thresholds. The controller leaves CV mode only when the terminal voltage or SOC drops below their limits by a set amount. This approach keeps the mode stable. While in CV mode, a proportional–integral (PI) controller sets the charging current based on the voltage error. This lets the current decrease smoothly as the battery nears full voltage. A minimum current limit is set to avoid very low current near the end of charging.

```
%% ---------------- Tunables ----------------
Ts         = 1e-5;      % controller sample time [s] [1/(10*rectifier.SwitchFrequency)]
SOC_th     = 0.879;      % SOC threshold for CV entry
SOC_hys    = 0.01;      % SOC hysteresis
V_hys      = 5.0;       % voltage hysteresis [V]

% CV taper PI gains (start gentle)
Kp_cv      = 0.4;
Ki_cv      = 15.0;

% Minimum current at end of charge
I_min_frac = 0.005;     % 0.5% of rated current

% Slew-rate limiting for smooth current transition
slew_Aps   = 50;      % A/s (reduce more if taper is still too fast)

%% ---------------- Derived ----------------
I_min  = I_min_frac * Icc_ref;
dI_max = slew_Aps * Ts;

%% ---------------- Persistents ----------------
persistent mode int_v Iprev
if isempty(mode),  mode  = false; end   % false=CC, true=CV
if isempty(int_v), int_v = 0.0;   end
if isempty(Iprev), Iprev = Icc_ref; end

%% ---------------- Mode Logic ----------------
% Enter CV only when BOTH conditions are true
if ~mode
    if (Vbat >= Vcv_ref) && (SOC >= SOC_th)
        mode = true;
    end
else
    % Exit CV only if either variable falls back enough
    if (Vbat <= (Vcv_ref - V_hys)) || (SOC <= (SOC_th - SOC_hys))
        mode = false;
    end
end
```

**Figure 3-10**: CC to CV Transition

A slew-rate limiter is also used on the current reference to make sure changes between modes happen gradually. This reduces stress on the converter and makes simulations more reliable.

### 3.4.2 Protection and Supervision Layer

A protection supervision module acts as a top-level control to keep the megawatt charging system safe and reliable, following IEC 61851-23-3 requirements as shown in **Figure 3-11**. It uses voltage and current limits that match the real operating boundaries of high-power DC charging systems. A very detailed algorithmic code can be seen in **Appendix G — Protection and Supervision Algorithm**

```
%% ================= Tunable parameters =================
Ts = 1e-5;    % controller sample time [s]

% -------- Side B voltage logic (MCS) --------
Vbat_max_normal      = 1250.0;   % normal maximum negotiated side-B voltage [V]
Vbat_emergency_trip  = 1375.0;   % emergency shutdown threshold [V]

% -------- DC bus protection --------
Vdc_min_connect      = 1100.0;   % minimum DC bus voltage before closing switch [V]
Vdc_max_warn         = 1250.0;   % start limiting / warning region [V]
Vdc_emergency_trip   = 1375.0;   % hard trip threshold [V]

% -------- Current protection --------
Ibat_max_limit       = 1400.0;   % charging overcurrent trip [A]

% -------- Timing --------
t_startup_blank      = 0.05;     % ignore all faults during initial startup [s]
t_bus_stable         = 0.03;     % wait before closing switch [s]
t_post_connect_blank = 0.03;     % ignore normal faults after closing switch [s]
t_fault_debounce     = 0.003;    % normal fault debounce [s]
t_emergency_debounce = 0.001;    % emergency fault debounce [s]

% -------- Safe shutdown --------
ramp_down_Aps        = 5e4;      % ramp current down during controlled shutdown [A/s]
I_open_thresh        = 20.0;     % open switch only when current below this [A]
```

**Figure 3-11**: Protection and Supervision Parameters

The protection scheme constantly checks important system values like DC-link voltage, battery terminal voltage, and charging current. It uses a two-step voltage protection method: normal operation is limited to 1250 V, and emergency shutdown happens at 1375 V, matching IEC limits for high-voltage DC charging.

Besides voltage protection, the battery current is kept below 1400A to avoid overloading the battery and power electronics. If the charging current goes above this limit, the system takes protective action. This keeps the system safe during high-power charging and prevents overheating or electrical damage.

The DC-link is monitored to make sure the converter works properly. Power is only sent to the battery if the DC-link voltage is above a set minimum (1100V), which keeps the converter stable. High voltage limits help spot problems and trigger protection if needed. A coordinated timing strategy is implemented to differentiate between normal transient behavior and genuine fault conditions. During startup, a brief blanking period (~80ms) suppresses protection actions as the converter energizes and the DC-link stabilizes. A comparable delay is applied immediately after load connection to prevent nuisance tripping from expected transient responses. Additionally, debounce logic ensures that only persistent abnormal conditions trigger fault activation.

The protection system can do both controlled and emergency shutdowns. If the problem is not critical, it slowly lowers the charging current to reduce stress on the converter and battery. For serious faults, it shuts down right away to keep the system safe. The protection module works together with the CC–CV charging supervisor. The charging controller sets the target current, but the protection system can limit or change this value as needed, depending on real-time conditions. It mainly uses terminal voltage as feedback, so protection actions match how the battery is really behaving during charging. The protection logic described here is meant for normal operation. During grid disturbance tests like LVRT and OVRT, some protection features are adjusted or relaxed. This lets engineers test how the system behaves in unusual situations without causing unwanted shutdowns. This combined protection and supervision approach meets all relevant standards and handles the real challenges of high-power converter systems. It helps the megawatt charging system run smoothly and reliably.

### 3.4.3 DC-DC Converter Control Interface

The current reference generated by the supervisory controller is provided to the DC–DC converter control circuit. The converter regulates the output current accordingly as shown in **Figure** 3-12: DC-DC Control Circuit and generates switching signals for the power stage.

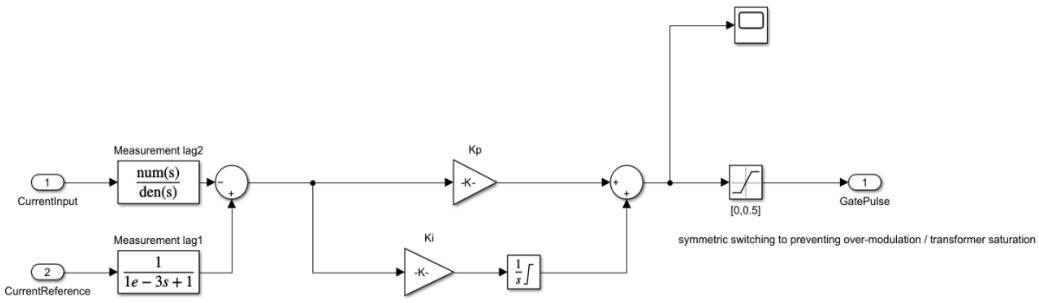


**Figure 3-12**: DC-DC Control Circuit

This layered architecture ensures clear separation between:

- High-level decision making (charging + protection)
- Low-level control (converter switching)

## 3.5 System-Level Operation

The overall system operates through coordinated control of the grid-side and battery-side converters, with a clear functional separation between the active front-end (AFE) and the DC–DC conversion stage. The AFE manages grid interaction, such as synchronization, current injections, and DC-link voltage regulation. Using grid-following vector control, it ensures controlled power transfer from the grid and keeps power quality and stable operation even when grid conditions change.

The DC-DC converter controls battery charging by adjusting the output-current based on a reference signal from the supervisory control layer. This stage accurately follows

the CC-CV charging profile, keeps electrical isolation, and delivers power to the battery in a controlled way.

Separating these responsibilities allows the grid-side and battery-side control loops to be tuned independently. This helps the system stay stable under many operating conditions, even when grid strength changes or there are disturbances at the point of common coupling.

## 3.6 Performance Evaluation Technique

An automated evaluation technique was created in the simulation environment to study how the charging system behaves under real-world conditions. This system calculates key performance indicators for both power quality and charging performance.
The primary evaluation metrics consist of:

- Grid current total harmonic distortion (THDi)
- DC-link voltage ripple
- Battery voltage ripple
- Battery current ripple
- IEC-aligned ripple metrics based on frequency-dependent limits

The system is evaluated under a set of standardized test conditions designed to reflect grid-code-oriented scenarios, including:

- Low-voltage ride-through (LVRT) and overvoltage ride-through (OVRT) events
- Steady-state voltage variations of ±10%
- Off-nominal frequency conditions

These test cases allow systematic analysis of converter behavior, control stability, and power quality performance over various grid conditions. This evaluation technique is the foundation of the Grid-Integrated MCS Validation Framework (GMVF) approach adopted

in this work. It enables repeatable and structured testing of megawatt-scale charging systems without needing physical prototypes, while still meeting grid-code requirements.

## 3.7 Power Quality and Ripple Evaluation Methodology

The performance of the charging system is evaluated using a structured signal-processing methodology applied to simulation data, designed to reflect both methodical rigor and practical measurement considerations encountered in high-power converter systems.

In industrial environments, power quality assessment is inherently influenced by switching transients, measurement noise, and control-induced oscillations. To ensure meaningful evaluation, all signals get processed after a predefined time threshold corresponding to quasi-steady-state operation. This avoids distortion of results due to startup behavior, DC-link charging dynamics, and controller settling.

For ripple analysis, a steady-state monitoring window of 0.2 s is selected at the end of the simulation. This duration is intentionally chosen to ensure adequate resolution of low-frequency components, particularly around 10 Hz, that are necessary from a battery stress perspective. Shorter windows may underestimate low-frequency ripples, leading to misleading conclusions.

### 3.7.1 Grid Current THD Evaluation

Grid current quality is evaluated using Total Harmonic Distortion (THD) based on frequency-domain analysis. To guarantee robustness comparable to practical measurement systems, the signal is first resampled onto a uniform time base, then the DC component is removed, and a Hann window is applied to diminish spectral leakage. Please note that harmonics are extracted from EMT time-domain waveforms using FFT and expressed as RMS-based THD values

A Fast Fourier Transform (FFT) is then performed, and harmonic components are extracted within narrow frequency bands around integer multiples of the fundamental frequency. This band-limited approach improves accuracy in the presence of frequency deviations and spectral-based spreading, that are common in converter-driven systems.
The calculated THD is further cross-validated using MATLAB's built-in thd() function, guaranteeing consistency and reliability of the harmonic assessment.

**Time-Domain Ripple Metrics**

Initial ripple characterization is performed using peak-to-peak values within the steady-state window. Ripple is expressed as a percentage of the average value and evaluated for DC-link voltage, battery terminal voltage, and battery current.
While this strategy provides a clear indication of fluctuation magnitude, it does not distinguish between low-frequency and high-frequency components, which have significantly different physical impacts on system performance and battery degradation.

### 3.7.2 IEC Aligned Battery Current Ripple Analysis

To address this limitation, an IEC-aligned ripple evaluation methodology is implemented that reflects the frequency-dependent nature of battery stress.

The battery current is decomposed into its average (DC) and oscillatory (AC) components by subtracting the mean. The resulting AC component is then passed through first-order low-pass filters with cut-off frequencies of 10 Hz, 5 kHz, and 150 kHz.

This filtering approach corresponds to the intent of IEC standards, which do not evaluate ripple as a single aggregated value but rather as frequency-dependent components.
**Each frequency band represents different physical phenomena as follows:**

- Low-frequency ripple (~10 Hz): associated with control dynamics, grid interaction, and DC-link oscillations

- Mid-frequency ripple (~5 kHz): influenced by converter interaction and switching harmonics
- High-frequency ripple (~150 kHz): dominated by switching transitions and parasitic effects

The filtered signals are evaluated using both peak-to-peak and RMS values, normalized with respect to the average charging current, and compared against IEC-defined limits as shown in **Figure 3-13**.

**101.1.5 Periodic and random deviation (current ripple at side B during CCM)**

IEC 61851-23:2023, 101.1.5 is applicable, except as follows:

*Replacement of "Table 118" by "Table 205 of IEC 61851-23-3:202X".*

**Table 205 – Current ripple limit of the EV supply equipment**

| Frequency [a] | Present current at side B (I) (limit in percentage of the maximum value of that range and absolute value as $A_{peak\text{-}to\text{-}peak}$) | |
|---|---|---|
| | I ≤ 200 A DC | 200 A DC < I |
| 10 Hz | 1,5 | I x 0,75 % |
| 5 kHz | 6,0 | I x 3,0 % |
| 150 kHz | 9,0 | I x 4,5 % |
| [a] Cut-off frequency of the first order low pass filter. | | |

**Figure 3-13:** Ripple Limits as per IEC 61851-23-3 clause 101.1.5

A sampling feasibility check is included to ensure the simulation sampling rate is sufficient to capture higher-frequency components. If the sampling resolution is inadequate for a given frequency band, the corresponding result is flagged as invalid, reflecting realistic measurement boundaries.

### 3.7.3 Practical Considerations

The technique itself is employed in a simulation environment based on Simscape software, which simulates the physical system behavior at the circuit level. Such an approach permits the simulation model to account for realistic system behavior effects such as switching, converter behavior, and transient processes, thereby providing an accurate estimation of system performance.

However, some practical features of measuring systems are not considered within the framework of the simulation model. First of all, high-frequency ripple measurements cannot be carried out without accounting for various factors, including restrictions imposed by sensors and data collection hardware and noise. The simulation model produces highly detailed signals, maybe resulting in overly positive estimations compared to measurements performed in practice.

Digital filtering employed for ripple measurement approximation in compliance with IEC standards may not perfectly reflect the process of signal processing in hardware systems. In turn, the estimation of low-frequency ripple requires selecting the proper measurement window depending on the signal frequency, particularly when signals with frequencies close to 10 Hz are involved. Nevertheless, the selected methodology guarantees realistic and accurate results of system performance estimation.

# 4 Results and Discussions

This chapter covers the performance evaluation of the proposed megawatt charging station under various conditions. The analysis of the obtained results is carried out from the perspectives of power quality, control stability, and interaction with the power grid, with comparisons made based on different configurations of the converters and grid conditions.

## 4.1 Introduction

In this chapter, the results of the development of the megawatt-level electric vehicle charging station have been presented. The analysis is performed within the framework of the GMVF approach discussed in Chapter 3, providing for consistent modeling, controller design, and system analysis.

The purpose of this chapter is to investigate the electrical performance, control stability, and power quality properties of the charging system, paying special attention to grid interactions and battery side performance under megawatt power levels. This investigation is conducted for both stable and disturbed modes of operation to simulate real-world conditions of the power system.

The assessment includes the investigation of the influence of different grid strength values (strong, medium, and weak grid), sensitivity to different charging currents, and reaction to different grid variations such as voltage sag, voltage swell, and frequency deviation. Moreover, dynamic behavior has been investigated in ride-through situations, including low-voltage and high-voltage-ride-through.

In addition, battery-side performance has been analyzed not only with respect to classical ripples but also in the context of modern standards, such as IEC 61851-23-3, which allows estimating the influence of current ripples on battery stress.

Results are not only relied on numerical data but also on physical phenomena such as the interaction between grid impedance and converters, dynamics of control, and modulation. This way, the overall performance can be evaluated. Additionally, the operation of MW charging stations according to the grid code can also be assessed.

## 4.2 IEC 61851-23-3- Based Validation and Initial Compliance Assessment

Initially, the designed megawatt charging system will be validated for its performance and compliance with the requirements defined in IEC 61851-23-3. Such validation will serve as the starting point for the assessment of the developed charging system before analyzing its dependence on the grid.

Specifically, the following three aspects will be considered during the validation process:

- Satisfaction of the frequency-dependent current ripple requirements specified in IEC **(primary requirement**)
- Control of the system's energization and reliable energy transfer
- Correctness of the implemented CC-CV charging algorithm that depends on the terminal voltage

### 4.2.1 System-Level Functional Validation

The stability of energy transfer in the proposed method is demonstrated via protection and sequencing strategies employed in the scheme. A delay of 80 msec in start-up is initiated to stabilize the DC-link before connecting to the loads, which prevents any transient inrush and switching effects during load connection from influencing system operation same can be witnessed in **Figure 4-2** .

Steady-state energy delivery to the battery after initialization is achieved. The DC-link voltage is controlled to be near its nominal value (≈1200 V). In addition, the battery is charged via constant current mode at a certain C-rate (1.65 C).

The CC/CV charging algorithm performs effectively since the transition process depends on the terminal voltage and state-of-charge of the battery. Terminal voltage guarantees

a precise representation of the battery performance while open-circuit voltage causes unnecessary switching to the constant voltage mode, which is undesirable. In normal operation mode, no protection is required due to the absence of any overvoltage/over-current phenomena in the DC-link and the battery terminals.

### 4.2.2 IEC-Aligned Battery Current Ripple Evaluation – Initial Results

Ripple currents in the battery are measured according to the procedure stated in Chapter 3, which utilizes first-order low-pass filters operating at frequencies of 10 Hz, 5 kHz and 150 kHz to filter the ripple current. This filtered ripple is then compared to limits as per IEC standards (IEC 61851-23, 2024) for high current charging systems. A representative result for the weak grid condition (SCR = 3) for 3-Level converter is presented in **Figure 4-1**.

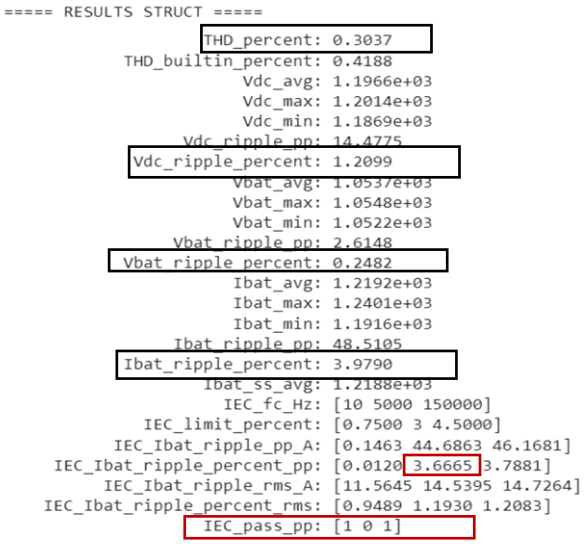


**Figure 4-1**: IEC-Aligned Battery Current Ripple Evaluation Showing Mid-Frequency Non-Compliance for SCR=3, 3-Level Converter

As we can see in **Figure 4-1**, the system satisfies IEC limits in the 10 Hz and 150 kHz bands but exceeds the IEC limit in the 5 kHz band.

**Based on numerical analysis, it can be stated that:**

- Low-frequency ripple (10 Hz band) is below the IEC limit
- High-frequency ripple (150 kHz band) also satisfies the IEC limit
- Middle-frequency ripple (5 kHz band) violates the IEC limit

For the present scenario, the ripple in the middle band (5 kHz) is around 3.66%, which is above the IEC limit of 3%. To verify the consistency of this behavior, the IEC ripple evaluation is extended across all tested configurations, as summarized in **Appendix B — IEC-Based Battery Current Ripple Evaluation**, and we found that violation in every test.

### 4.2.3 Interpretation of Initial Compliance Behavior

The results of the IEC-based assessment show a steady and systematic pattern under all test cases.

- Compliance with the ripple constraint at low frequencies (10 Hz)
- Also, compliance with the high-frequency ripple (150 kHz)
- There is a regular non-conformity at mid-frequencies (5 kHz)
-

**These results are regardless of:**

- Grid strength (SCR = 3, 5, 12)
- Inverter design type (Average, 2-Level, 3-Level)

The consistent nature of the non-conformity shows that the cause of the problem is not connected to the grid-side dynamics or the converter topology at the active front-end. Rather, the problem lies in the internal dynamics of the battery-side conversion stage.

### 4.2.4 System Behavior under Non-Compliant Conditions

Although the IEC ripple requirement is not satisfied in the mid-frequency band, the overall system remains stable and operates as intended from a control and energy transfer (~80 msec) perspective. The time-domain response of the system under the same weak grid condition is shown in **Figure 4-2**.

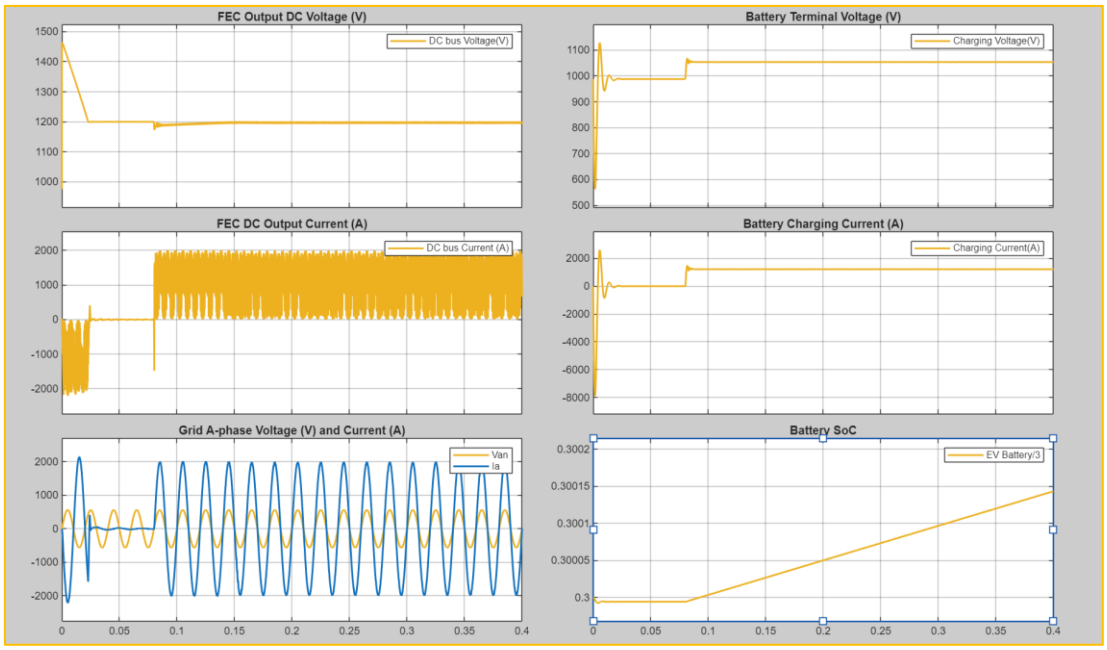


**Figure 4-2**: Time-Domain Response of the Charging System under Weak Grid Condition (SCR = 3, 3-Level Converter)

DC-link Voltage, Battery Voltage, Charging Current, and grid voltage waveforms showing stable performance with controlled energy conversion even in the presence of mid-frequency ripple components.

**These waveforms in Figure 4-2 clearly show that:**

- DC link voltage is under stable regulation
- Battery voltage has smooth behavior
- Charging current is under stable control
- Proper grid voltage synchronization

From this, we conclude that the IEC non-compliance is not because of stability or control issues but due to inadequate filtering of certain frequency components from the battery current.

### 4.2.5 Implications for System Design

Firstly, the validation result of the IEC indicates that:

- The system fulfills all functional requirements regarding energy transfer, control, and protection
- Performance on the grid side is consistent and not the constraint
- Unfortunately, the basic design fails to meet the full standards set by the IEC for ripple.

Mainly, the problem resides in the medium frequency ripple (~5 kHz) which could not be attenuated properly by the battery side filter.

**Consequently, one important finding is:**

It is difficult to meet the requirements of IEC 61851-23-3 only through the design or choice of parameters. This requires proper control of the system dynamics, especially inside the battery-side converter and filter section.

### 4.2.6 Transition to Sensitivity Analysis

Considering the systematic occurrence of this ripple problem for mid frequency range, further study is needed to pinpoint the key factors contributing to the problem and develop an appropriate mitigation technique. Therefore, a sensitivity and parameter study will be conducted in the subsequent section, which is intended to solve the identified problem and ensure full compliance with IEC 61851-23-3 standards.

## 4.3 Sensitivity Analysis and Design Refinement

Following the observed IEC non-compliance in the 5 kHz ripple band, a targeted sensitivity analysis was conducted to identify the dominant parameters influencing battery current ripple and to determine feasible mitigation strategies within real design constraints.

### 4.3.1 Problem Focus: Mid-Frequency Ripple (5kHz)

As system consistently exceeds the IEC ripple standard within the 5 kHz range regardless of the strength of the grid connection and inverter topology. This implies that the problem lies in the battery side power conversion stage and not in the grid interaction stage.

Considering that ripple transmission at the battery interface is controlled by the output filter and switching dynamics, the investigation is based on:

- DC-DC converter switching frequency
- Output filter inductor and capacitor values
- Damping characteristics of the LC filter

### 4.3.2 Influence of Output Inductance

The output inductance serves as a critical factor for determining the current ripple in the battery due to its ability to smooth out variations in the current at the output of the DC/DC converter. It can be illustrated in equation 4.1 that there exists the following relationship between the ripple, the inductance, and the switching frequency:

$$\Delta I \propto \frac{1}{L \cdot f_{sw}} \tag{4.1}$$

where $\Delta I$ is the current ripple, $L$ is the output inductance, and $f_{sw}$ is the switching frequency.

However, in the current design, the value of the inductance is limited in accordance with the IEC 61851-23-3 to keep its value below 100 µH to provide safety under short-circuit conditions. Thus, the output inductance was chosen very close to this upper limit (≈99 µH) to maximize passive ripple attenuation.

**Nevertheless, according to the results obtained in Section 4.2, we have found that:**

- mid-frequency ripple (~5 kHz) still remains dominant
- IEC ripple limits are still violated

This indicates that, under practical constraints, inductance alone cannot ensure compliance.

### 4.3.3 Influence of Switching Frequency

By keeping the inductance around the IEC boundary condition, the switching frequency range between 10 kHz and 45 kHz is analyzed to determine the effect of ripple in the system. Based on the analysis results, the following conclusions can be drawn:

- considerable improvement in ripple suppression between 10 kHz and 20 kHz
- moderate improvement until 30 kHz
- saturation after 35-40 kHz, showing no further improvements

As explained in equation (4.1) under section 4.3.2, an increase in switching frequency causes a decrease in ripple, as the harmonics are shifted towards higher frequencies. However, once the dominant resonance boundary is passed, the system reaches its saturation point, where further improvements are not possible.

Furthermore, a high switching frequency causes high switching losses and temperature, rendering the process inefficient without using other techniques. Therefore, switching frequency scaling alone is insufficient to resolve the 5 kHz ripple non-compliance and we decided to keep the switching frequency of our DC-DC converter is at 40kHz.

### 4.3.4 Influence of DC Link Capacitance

The impact of DC-link capacitance on load side ripple behavior was also evaluated. Increasing capacitance improves DC-link voltage stability but has limited influence on battery current ripple, particularly in the mid-frequency range.

Furthermore, larger capacitance values introduce increased system stiffness and may shift ripple effects toward the load side rather than eliminating them. This confirms that DC-link capacitance is not the dominant factor governing IEC ripple compliance. Analysis says that optimization is the key to DC capacitor sizing, not maximization; adequate capacitance helps in stabilization of Vdc, but too much rigidity or reduction might cause problems in terms of power quality, synchronization and control interaction can be seen in attached **Appendix E — DC Bus Link Capacitance**.

### 4.3.5 Necessity of Damping for IEC Compliance

The overall sensitivity analysis shows that:

- Inductance depends on IEC safety limits,
- Further increase of switching frequency yields diminishing returns, and
- The effect of DC link capacitance on battery current ripples is relatively low.

In turn, the dominating issue becomes LC resonance in the output filter that causes an amplification of ripple frequencies at the mid-range (~5 kHz). Therefore, the approach to tackle this problem was to incorporate a damping resistor (0.027 Ω) into the output filter in series with capacitor, which helped to:

- Eliminate LC resonance,
- Damp the oscillations in the mid-range, and
- Stabilize the current without exceeding IEC limits.

As a result, the introduction of damping becomes the critical step in reducing the main ripple component in order to achieving IEC-compliant operation.

## 4.4 Successful IEC Compliance after Design Optimization

Upon determining that the ripple band at 5 kHz is the most significant source of failure for IEC compatibility, the output filter on the battery side was improved through the addition of damping into the capacitor branch. The optimized filter uses the following parameters: damping resistor equal to 0.027Ω, battery side inductance of 99µH, while the battery-side output capacitance was retained at $15\ \mathrm{mF}$, within the estimated design range of approximately 10–15 mF. These values have been chosen because they eliminate the mid-frequency oscillation effect without exceeding the capacitance requirement.

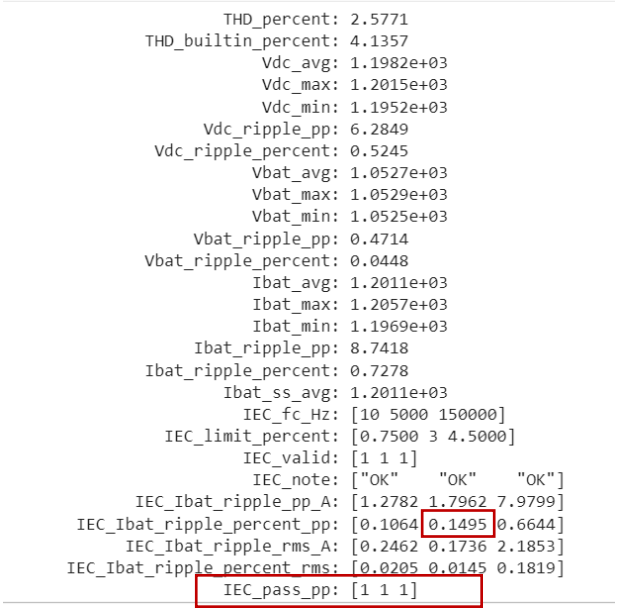


**Figure 4-3**: – IEC-Compliant Battery Current Ripple after Addition of Damping (SCR = 3, 3-level converter)

Above **Figure 4-3** is an analysis of ripple content after the introduction of damping resistance within the battery side output filter. All three bands analyzed satisfy IEC requirements for ripple content – 10 Hz, 5 kHz, and 150 kHz.

Also, we can say that the ripple frequency band that was originally out of tolerance has been brought back to an acceptable value, while the rest remained within their respective requirements. Thus, the initial problem was not caused by the lack of capacitance but by the inadequacy of the damping mechanism, which eventually helped the system to pass in all cases as shown in **Appendix C — IEC-Based Battery Current Ripple Evaluation.**

### 4.4.1 Design Outcome

The final battery-side filter and battery configuration used for IEC-compliant operation is summarized in **Table 1**.

**Table 1**: Final Battery-Side Parameters after Design Optimization

| Parameter | Final value |
|---|---|
| Battery damping resistor | $0.027\ \Omega$ |
| Battery-side inductance | $99\ \mu H$ |
| Battery-side output capacitance | $15\ mF$ |

This result establishes damping as the critical design refinement required to achieve IEC-compliant battery current ripple in the developed megawatt charging system.

## 4.5 Grid Strength and Power Quality Performance

Performance assessment of grid strength effects is conducted using different values of short-circuit ratio SCR (12, 5, 3), where the X/R ratio is fixed at 10, all other parameters of design and control were kept fixed. The comparisons are made among Average model, 2-Level inverter, and 3-Level inverter topologies. Power quality parameters considered for assessment are grid current THD, DC-link voltage ripple, battery current ripple, and battery voltage ripple.

### 4.5.1 Power Quality Metrics under varying Grid Strength

Below tables are the KPI values noted while changing the grid characteristics and converter topology and keep all other parameters unchanged, for consistency of comparative analysis.

**Table 2**: Power Quality Performance of Average Model under Varying Grid Strength

| Case | SCR | X/R | THD (%) | Vdc Ripple (%) | Ibat Ripple (%) | Vbat Ripple (%) |
|---|---|---|---|---|---|---|
| Strong Grid | 12 | 10 | 0.250 | 0.054 | 0.725 | 0.045 |
| Moderate Grid | 5 | 10 | 1.697 | 0.217 | 0.728 | 0.045 |
| Weak Grid | 3 | 10 | 7.264 | 0.518 | 0.725 | 0.045 |

**Table 3**: Power Quality Performance of 2-Level Inverter under Varying Grid Strength

| Case | SCR | X/R | THD (%) | Vdc Ripple (%) | Ibat Ripple (%) | Vbat Ripple (%) |
|---|---|---|---|---|---|---|
| Strong Grid | 12 | 10 | 2.299 | 0.1218 | 0.7306 | 0.045 |
| Moderate Grid | 5 | 10 | 2.783 | 0.259 | 0.728 | 0.045 |
| Weak Grid | 3 | 10 | 3.177 | 0.525 | 0.722 | 0.044 |

**Table 4**: Power Quality Performance of 3-Level Inverter under Varying Grid Strength

| Case | SCR | X/R | THD (%) | Vdc Ripple (%) | Ibat Ripple (%) | Vbat Ripple (%) |
|---|---|---|---|---|---|---|
| Strong Grid | 12 | 10 | 1.581 | 0.108 | 0.729 | 0.045 |
| Moderate Grid | 5 | 10 | 3.047 | 0.2318 | 0.728 | 0.0448 |
| Weak Grid | 3 | 10 | 2.577 | 0.525 | 0.728 | 0.045 |

The results in **Table 2**, **Table 3** and **Table 4** show a clear dependence of grid side performance at PCC on grid strength. Grid current THD shows a substantial increase when the strength of the grid reduces. In terms of the Average case, the value of THD increases from 0.25% at SCR 12 to 7.26% at SCR 3. The same pattern is evident for both inverter cases but with lower absolute values. On weaker grids, the 3-Level inverter has a THD of 2.577%, while the 2-Level inverter has 3.177%, indicating better harmonic performance for 3-Level inverter has been observed under weak grid.

DC-link voltage ripples also increase with decreasing grid strength. For example, in the 3-Level inverter case, ripple increases from 0.108% (strong grid) to 0.525% (weak grid). This reflects the reduced grid stiffness, which results in larger voltage fluctuations at the point of common coupling. On the other hand, battery side parameters are not significantly influenced by the status of the grid. The ripple in the battery current is maintained at low values between 0.72% to 0.73% for all cases, while the ripple in the battery voltage is maintained at a low value of 0.045%. And it shows that DC-DC converter and output filter is effectively isolating battery from upstream disturbances.

### 4.5.2 Discussion of Results

From the above results, it can be noted that grid strength mainly affects grid-side power quality issues, such as harmonic distortion, as well as DC-link behavior, due to the high grid impedance levels encountered in weak grids.

When comparing different topologies, it is found that the 3 Level Inverter has a lower THD than the 2-Level Inverter because it has the capability of generating stepped voltages without significant harmonic content. The performance of the battery side remains the same irrespective of whether the grid is strong or weak and what topology of AFE has been selected. Therefore, the battery charging system experiences decoupling from grid disturbances.

### 4.5.3 Key Implication

The grid strength greatly affects the power quality of the grid side, whereas battery-side operations are not affected much because of the isolation created by the DC-DC converter. Also, in the case of a weak grid, poor voltage stiffness caused by the high impedance leads to distorted PCC voltage, affecting PLL phase locking.

## 4.6 Influence of DC Bus Operating Point on THD

To analyze the impact of operating point on the quality of the supply side, a sensitivity analysis was conducted where the DC bus current decreased from 2000 A (approximately 2.4 MW) to 1500 A (approximately 1.8 MW). This analysis was done mainly for weak-grid conditions (SCR ≈ 3) using the average value model, two-level (2L), and three-level (3L) converters. From the analysis of the outcomes in **Appendix D — THD vs DC Bus Rating** , it can be concluded that THD depends on the DC side operating point, while all other parameters such as the configuration and control of the system do not change. The decrease in the value of the current causes the lowering of the modulation index and, accordingly, affects the switching process and reduces the efficiency of harmonic

suppression. Such an effect is especially noticeable for the 3L inverter because THD deterioration occurs at the new level of the current.

More importantly, irrespective of the changes on the grid side of THD, there is no impact on the metrics for DC-side ripple content, which means that the DC-link and output filters still have successfully achieved decoupling of the load side from the grid side.

The above results illustrate the impact of the operating point on the performance of the converters along with the grid strength and topology. In 3L converters, improved performance is seen with increased loading while in reduced loadings, their sensitivity increases. On the other hand, 2L converters provide a more reliable operation under different loadings due to their robustness. Detailed quantitative comparisons for each converter topology are provided **in Appendix D — THD vs DC Bus Rating**.

## 4.7 Performance under Voltage Variation (±10%)

System performance is assessed by evaluating its response to changes in grid voltage within the range of ±10%. This means that the variations in voltage occur between ±69 volts at time t=0 sec and onwards , meaning 621 volts in under-voltage and 759 volts in over-voltage condition applied right from very beginning. This measurement seeks to gauge the ability of the system to manage the DC link and power quality while operating in charge mode.

### 4.7.1 Response under Undervoltage (−10%)

The undervoltage condition in **Figure 4-4** represents a reduction in available grid-side voltage, leading to reduced power transfer capability and increased current demand to maintain the charging power.

Under this condition, a noticeable reduction in DC-link voltage is observed. The DC bus settles at approximately:

- **1102 V (weak grid)**
- **1115 V (moderate grid)**
- **1125 V (strong grid)**

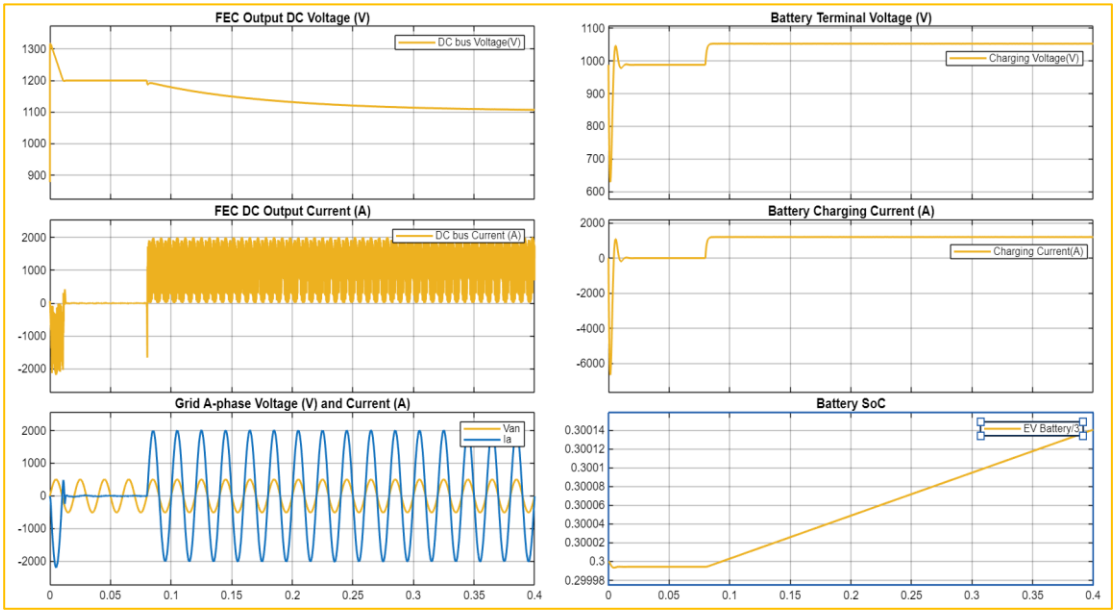


**Figure 4-4**: System Response under −10% Grid Undervoltage (Weak Grid Condition, 3 Level Inverter)

One can also notice that DC-link voltage control is highly dependent on the strength of the grid, leading to higher voltage fluctuations whenever the grid is weaker due to the presence of impedance.

Time-domain response in **Figure 4-4** showing DC-link voltage, grid current, battery voltage, and SOC under undervoltage operation. The decrease in the DC-link voltage causes an increase in the current stress of the converter as it works to compensate for the lower input voltage, as seen from the fluctuation and increase in magnitude of the grid current. It's been reflected in oscillatory behavior of grid current as well. Nevertheless, despite the foregoing, the battery side parameters have remained constant. Both the battery voltage and the charging current operating in required way, and the state of charge (SOC) keep changing dynamically. Overall System is performing

acceptable under deviated voltage condition, but active front end (AFE) is failing to regulate DC bus voltage at 1200 V, which again is acceptable considering the possibilities.

### 4.7.2 Response under Overvoltage (+10%)

The presence of overvoltage as in **Figure 4-5** causes more input voltage than required, which needs to be regulated by using the active front-end converter for smooth DC-link performance.

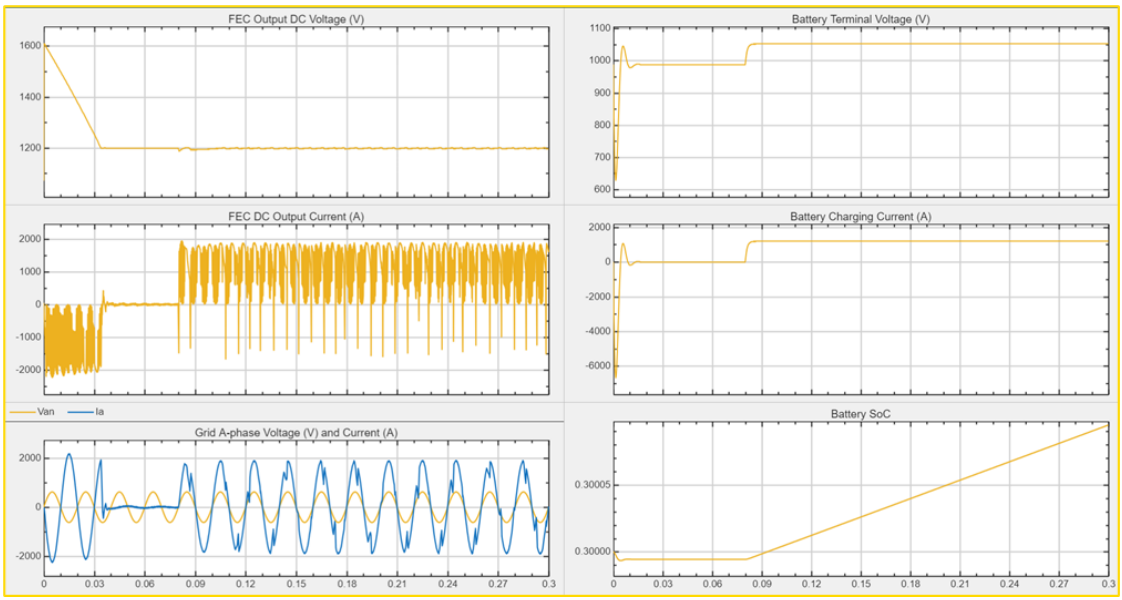


**Figure 4-5**: System Response under +10% Grid Overvoltage (Weak Grid Condition, 3 Level Inverter)

Time response graph in **Figure 4-5** demonstrating the regulation of the DC-link voltage, grid current response, and battery stability during overvoltage operation. Unlike undervoltage conditions where the voltage regulation becomes erratic, there is sufficient regulation of the DC-link voltage, which is set at about 1200V. This means that the surplus power will be sufficiently controlled, hence preventing overvoltage from propagating to the DC bus.

However, the level of harmonic distortion in the grid current rises when the system operates under overvoltage conditions. The harmonic distortion levels for the 3-level inverter are:

- **5.332% (weak grid)**

- **9.552% (moderate grid)**
- **2.195% (strong grid)**

The trend indicates that the combination of overvoltage with grid impedance effects has more significant impacts on the current waveform than DC-link voltage regulation.
Like the undervoltage scenario, battery side performance is relatively unchanged. Both the battery voltage and current stay constant, and there is no erratic behavior in the SOC profile.

### 4.7.3 Discussion

The analysis reveals that changes in voltage mainly affect grid side dynamics and control of DC link voltage, whereas the battery side dynamics are immune from such effects. In the case of low voltages, the DC link voltage decreases according to the degree of strength of the grid; therefore, highlighting the dependence of power transfer capability on the grid impedance. On the other hand, the high voltage does not affect the control of the DC link voltage but only leads to harmonic distortion of the grid voltage. It can be noted that under strong grid conditions, performance was good with respect to voltage stability and harmonic distortion. In contrast, weak grid conditions increase dynamic interactions leading to low DC link voltage (under-voltage condition) and high oscillations.

### 4.7.4 Important Observation

The under-voltage condition primarily affects the DC link voltage, while the over-voltage condition primarily affects the quality of the grid current.

## 4.8 Performance under Frequency Deviation (49 Hz)

The system performance is analyzed under off-nominal grid frequency for weak grid as **Figure 4-6** and for strong grid as **Figure 4-7**, particularly at 49 Hz where we connected EV station at time t=0 and battery load at 80 msec., to assess the grid-following controller's performance and its effects on power quality and DC-link voltage stability. This is

based on practical situations where there will be frequency changes due to generation/load mismatch.

### 4.8.1 Dynamic Response under Weak and Strong Grid Conditions

Time-domain responses from

**Figure 4-6** showing DC-link voltage, grid current, battery voltage, and SOC under frequency deviation for a weak grid (SCR = 3) are in stable condition.

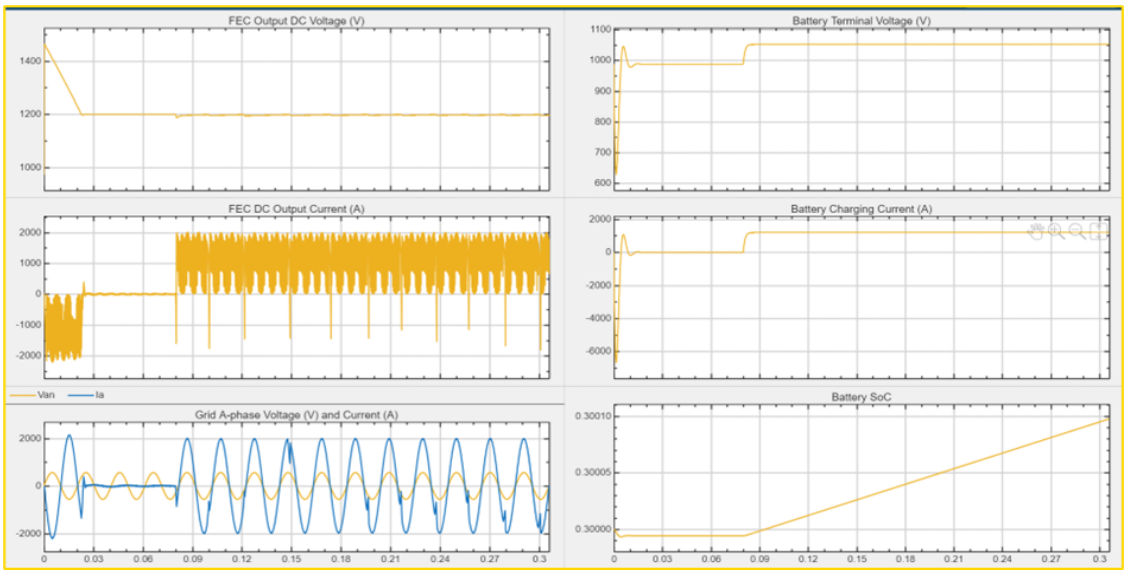


**Figure 4-6**: System Response under 49 Hz Operation (Weak Grid Condition)

Response in time domain from **Figure 4-7** showing behavior of the system at the same frequency deviation for the strong grid (SCR = 12) as well in stable condition.

In both cases, the system maintains synchronization with the grid using the phase-locked loop (PLL) during frequency deviation and operates continuously without losing control. Nevertheless, the responses vary depending on the strength of the grid.

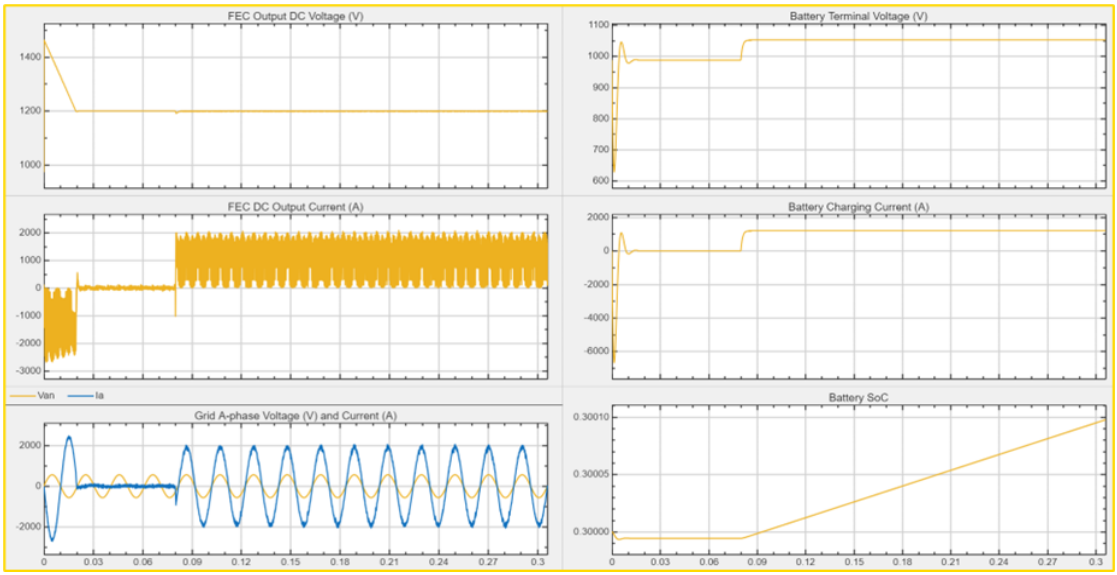


**Figure 4-7**: System Response under 49 Hz Operation (Strong Grid Condition)

For the weak grid configuration, there is an observable oscillation in the DC-link voltage, with slightly more ripples. In terms of grid current, there is distortion, suggesting an even stronger interaction between the grid and the converter. The percentage of grid current THD is around:

- **4.478% (weak grid)**

On the other hand, for the strong grid configuration, the DC-link voltage is stable with negligible ripples, while the grid current is smooth and almost sinusoidal in nature. The grid current THD is much lower at around:

- **1.041% (strong grid)**

From the results, it can be observed that changing the frequency alone will not lead to instability in the system, although its effect becomes stronger when there is a weak grid condition.

### 4.8.2 Power Quality Comparison

**Table 5**: Performance Comparison under 49 Hz Operation (3-Level Inverter)

| Parameter | Weak Grid (SCR = 3) | Strong Grid (SCR = 12) |
|---|---|---|
| Grid Current THD (%) | 4.478 % | 1.041 % |
| DC-Link Voltage Ripple (%) | 0.547 % | 0.103 % |
| Battery Voltage Ripple (%) | 0.044 % | 0.045 % |
| Battery Current Ripple (%) | 0.722 % | 0.727 % |

The results in

**Table 5** indicate:

- DC-link voltage regulation is somewhat less stable with high ripple in weak grids, but stable in strong grids.
- Grid current harmonics are considerably high in weak grids, indicating higher harmonic distortion.
- Battery side voltage and current ripples are low in both situations.
- System performance is limited by the grid in weak cases and is strong in strong grid cases.

### 4.8.3 Discussion

The obtained results prove that the system operates steadily in terms of frequency deviation, thus proving the feasibility of the grid-following method. In its turn, the PLL proves efficient at detecting non-nominal frequency and sustaining continuous synchronization and energy flow between the grid and load. As seen before, however, the strength of the grid remains one of the major factors influencing the performance of the system. In case of weak grid, lower short-circuit capacity leads to a greater sensitivity towards the frequency deviation, thus increasing the distortion of the currents and oscillation of the DC-link. An important feature of the results is that all battery-side parameters again remain stable regardless of frequency deviation.

### 4.8.4 Key Observation

Deviation in frequency does not affect system stability but significantly affects power quality, depending largely on the strength of the network, whereby a weaker network will show more oscillations and distortions.

### 4.8.5 Validation Note

The results obtained for both weak and strong grid systems at 49 Hz frequency are in accordance with the outputs of the simulation and analysis reports prepared throughout this study and is acceptable.

## 4.9 Low Voltage Ride-Through (LVRT) Performance

The performance of the proposed megawatt charger with respect to LVRT capability has been analyzed according to the voltage time criteria provided in EN 50549-2. The analysis confirms the capability of the charger to stay online during deep voltage sags, operate stably, and restore to the steady state condition post-fault for both 3 level and 2 Level inverters. The applied disturbance follows the standardized LVRT voltage–time envelope, including a voltage dip down to 0.05 p.u. and staged recovery. The reference characteristic shown below in **Figure 4-8** is as per EN50549-2.

**Figure 4-8** is showing a standard voltage profile defining the minimum voltage levels and duration for which the system must remain connected. The evaluation is based connectivity, stability during the fault, and post-fault recovery.

#### 4.5.3.2 Generating plant with non-synchronous generating technology

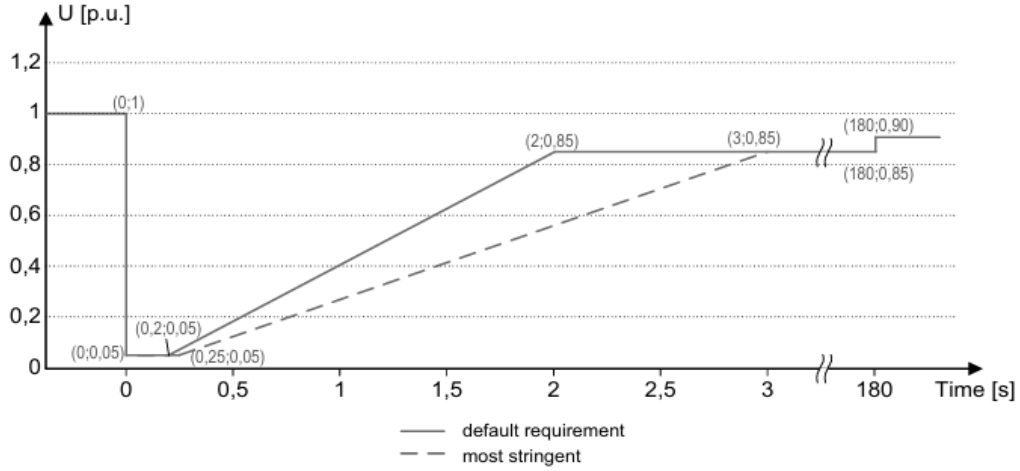


**Figure 4-8**: LVRT Voltage–Time Envelope as Defined in EN 50549-2

This research work generates a post process result to provide more insights on system performance while running through the ride through curves or grid dynamics as show in **Figure 4-9.**

```
Battery voltage remains valid          : PASS

Minimum Vbat during LVRT               : 976.81 V
Maximum Vbat during LVRT               : 1054.20 V


SOC remains physical and continuous    : PASS

Minimum SOC during LVRT                : 0.300003
Maximum SOC during LVRT                : 0.300603
Maximum adjacent SOC jump              : 0.000000









Remains connected during LVRT          : PASS

RECOVERY CHECKS
------------------------------------------------------------
Post-fault recovery                    : PASS
Recovered mean Vdc                     : 1192.51 V
Recovered mean Vbat                    : 1053.08 V
Recovered mean SOC                     : 0.300834
```

```
                LVRT SURVIVABILITY / REMAINS-CONNECTED REPORT
================================================================================
CASE INFORMATION
--------------------------------------------------------------------------------
Case name                              : LVRT Survivability Check
Nominal PCC line-line voltage          : 690.00 V
EVALUATION WINDOWS
--------------------------------------------------------------------------------
Startup ignored until                  : 0.080000 s
Pre-fault reference window             : 0.080000 s to 0.100000 s
LVRT active window                     : 0.100500 s to 3.100000 s
Recovery window                        : 3.100000 s to 4.100000 s
PRE-FAULT REFERENCE VALUES
--------------------------------------------------------------------------------
Mean pre-fault Vdc                     : 1195.70 V
Mean pre-fault Vbat                    : 1049.12 V
Mean pre-fault SOC                     : 0.299998


DURING-LVRT CHECKS
--------------------------------------------------------------------------------
DC bus survives                        : PASS
Minimum Vdc during LVRT                : 1099.19 V
```

```
OVERALL RESULT
------------------------------------------------------------------------------------------------------
LVRT survivability result              : PASS
NOTE
------------------------------------------------------------------------------------------------------
This result is based on simulation-based survivability logic using the applied
LVRT profile to define the disturbance window. Pass/fail is determined from
continued converter operation, battery-side validity, and post-fault recovery.
This is intended for engineering assessment only, not formal certification.

FAILURE REASONS / NOTES
------------------------------------------------------------------------------------------------------
1. None


======================================================================================================
END OF REPORT
======================================================================================================
```

**Figure 4-9**: LVRT Survivability Assessment Report, 3 Level, Weak Grid

Moreover, as per the post processed result obtained in **Figure 4-9** from simulation-based verification of DC-link stability, battery voltage validity, continuous operation, and successful recovery, it can be concluded that system met all the required conditions for LVRT as per EN50549-2.

Detailed visual inspection of the system response is also possible using the weakest grid scenario (SCR=3), as presented in the following figures:

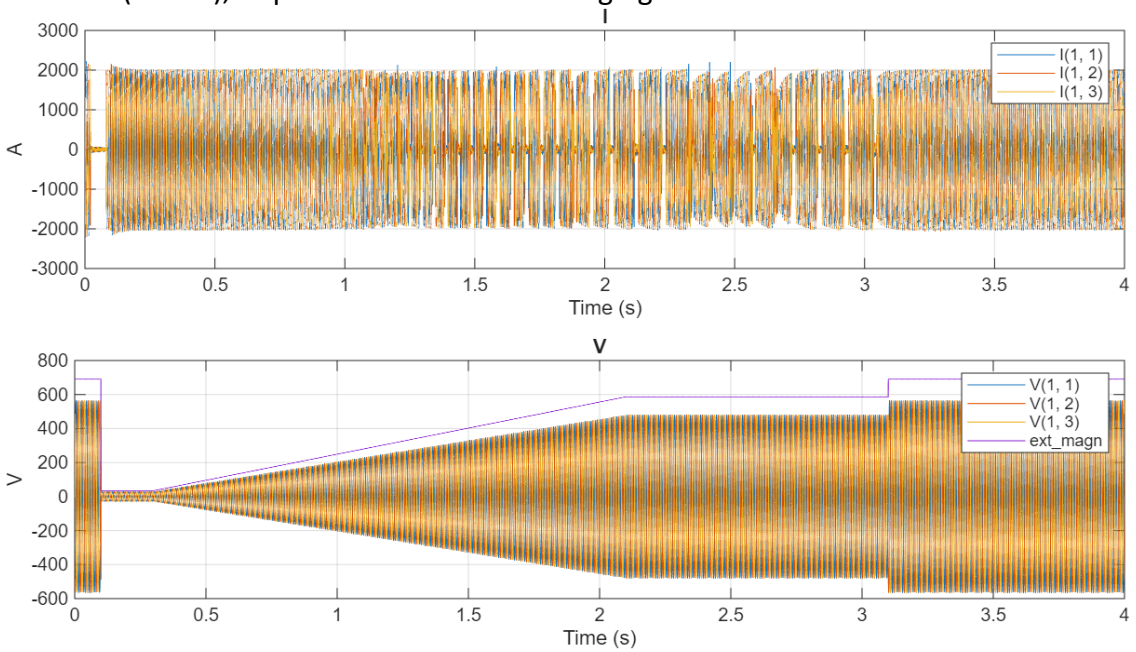


**Figure 4-10**: Three Phase Voltage and Current at Point of Common Coupling (PCC) under LVRT for Weak Grid (SCR=3), 3 Level Inverter

It can be observed that grid voltage in **Figure 4-10** adheres to the simulated LVRT profile, whereas grid current is distorted due to the fault and intense interaction between the converter and grid, yet system remains under control.

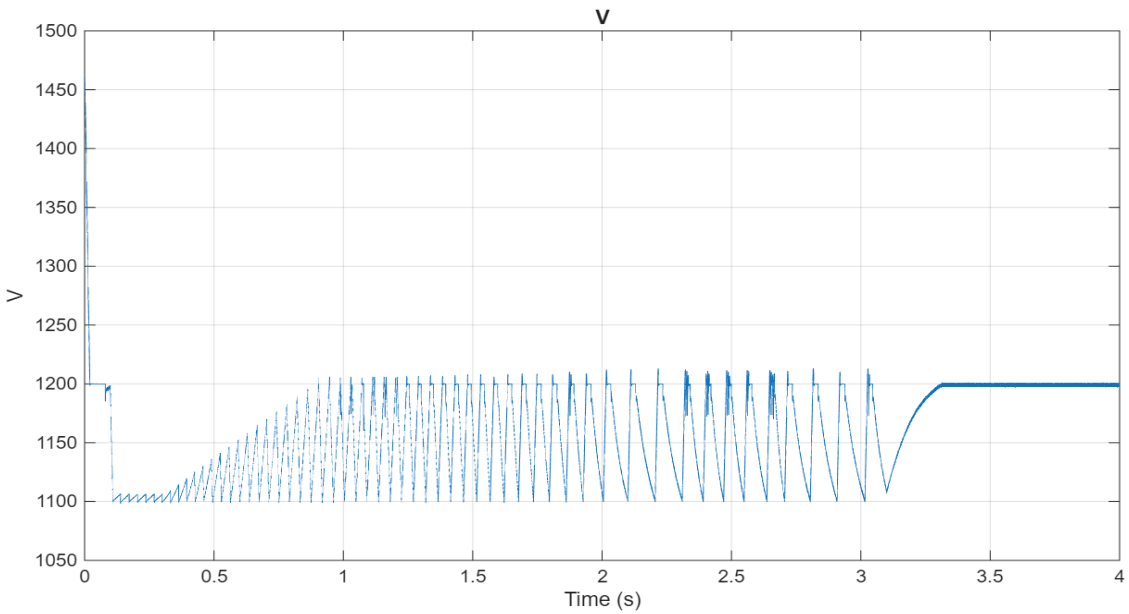


**Figure 4-11:** DC Link Voltage Profile under LVRT, Weak Grid, 3 Level Inverter

DC-link voltage in **Figure 4-11** shows a temporary drop and oscillatory behavior during the fault which is supporting the fact that active front-end (AFE) is trying harder to regulate the DC link voltage, yet remains bounded and recovers to nominal conditions and never let DC link voltage goes down and hit undervoltage trip condition set at 1100V.

The oscillations seen are mainly caused by the power mismatch between the AC and DC sides of the circuit in case of fault condition. The controller ensures power transmission is maintained despite the lack of voltage support provided by the grid.

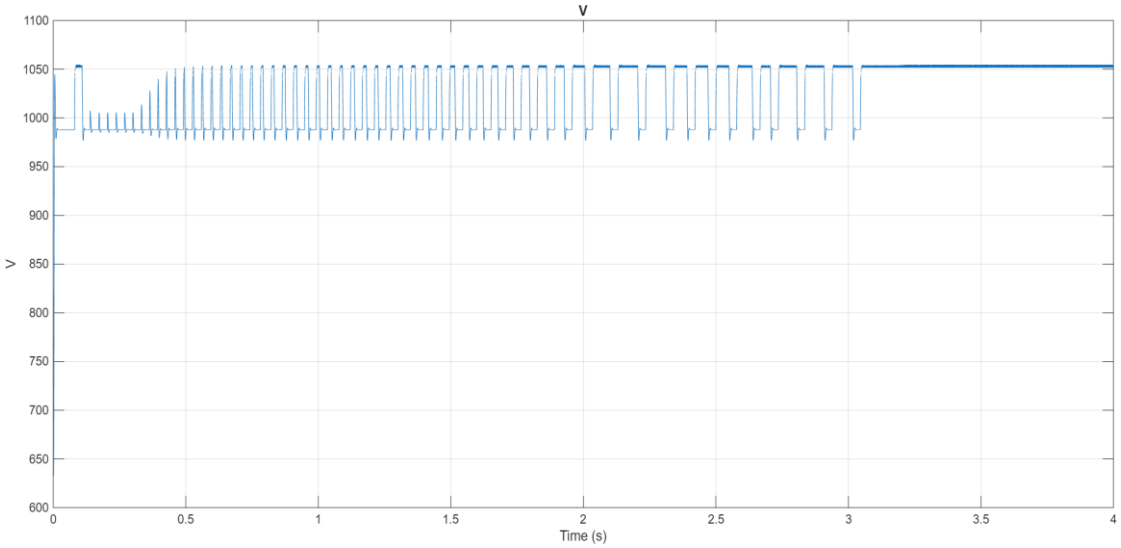


**Figure 4-12**: Battery Terminal Voltage during LVRT

Battery voltage in **Figure 4-12** remains within acceptable limits from 1100 V to 1250 V, indicating stable DC–DC converter operation.

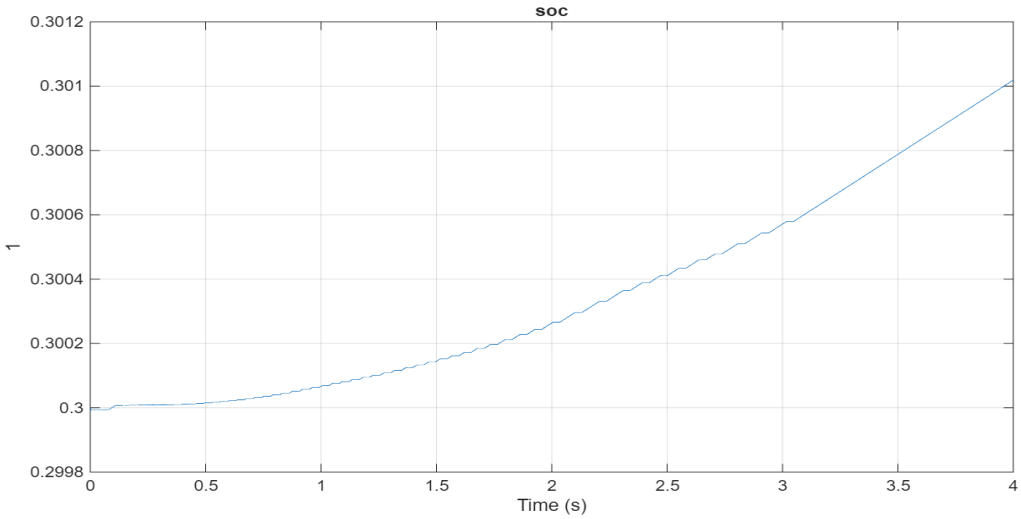


**Figure 4-13**: SOC Evolution during LVRT

As shown in **Figure 4-13** SOC is still continuous, meaning that there is no break in energy flow during the fault condition, which is solid proof of continuous operation. Thus, even in cases where the system exhibits high oscillation levels due to weak grid conditions, the system remains stable without disconnection.

### 4.9.1 Comparative Performance: 2-Level and 3-Level Inverters

To quantify system behavior, the 2-Level and 3-Level inverter systems will be examined using certain performance indices in LVRT conditions.

**Table 6**: LVRT Comparison Based on Key Power Quality Parameters

| Parameter | 2-Level Inverter (2L) | 3-Level Inverter (3L) |
|---|---|---|
| **LVRT Compliance** | Pass | Pass |
| **THD (Ia)** | 2.436 % | 0.716 % |
| **Vdc Ripple** | 8.960 % | 9.841 % |
| **Vbat Ripple** | 7.568 % | 7.577 % |

Based on the findings in **Table 6**: LVRT Comparison Based on Key Power Quality Parameters, it's clear that the both inverters (2-Level & 3-Level) meet the LVRT criteria, ensuring uninterrupted performance.

Nevertheless, variations in power quality occur during fault conditions:

- The 3-level inverter displays reduced current total harmonic distortion (THD) (≈0.716%) relative to the 2-level inverter (≈2.436%)
- Both systems show a rise in DC-link and battery ripples under fault conditions
- The ripple is considerably larger than at steady state due to fault effects

These observations highlight that LVRT compliance is achieved in both cases, but the dynamic quality of response differs between topologies.

### 4.9.2 Key Observation

A key outcome referring **Figure 4-8** to **Figure 4-13** is that LVRT compliance ensures system survivability and stability during faults but does not guarantee acceptable power quality under disturbed conditions. In general, the proposed control technique has been

shown to effectively meet the LVRT criteria set forth in standard EN 50549-2 under various operating conditions and for the two types of inverters (2L ,3L) considered.

## 4.10 Overvoltage Ride-Through (OVRT) Performance

The OVRT capabilities of the designed megawatt charger are tested according to the EN 50549-2 standard. It aims to ensure that the charger does not disconnect during voltage swell conditions and works under controllable conditions and within the required protection limits. The applied OVRT disturbance follows the voltage–time envelope specified in the standard, consisting of staged voltage increases up to 1.25 p.u., followed by gradual reduction to nominal conditions. The reference envelope used for evaluation is shown in **Figure 4-14.**

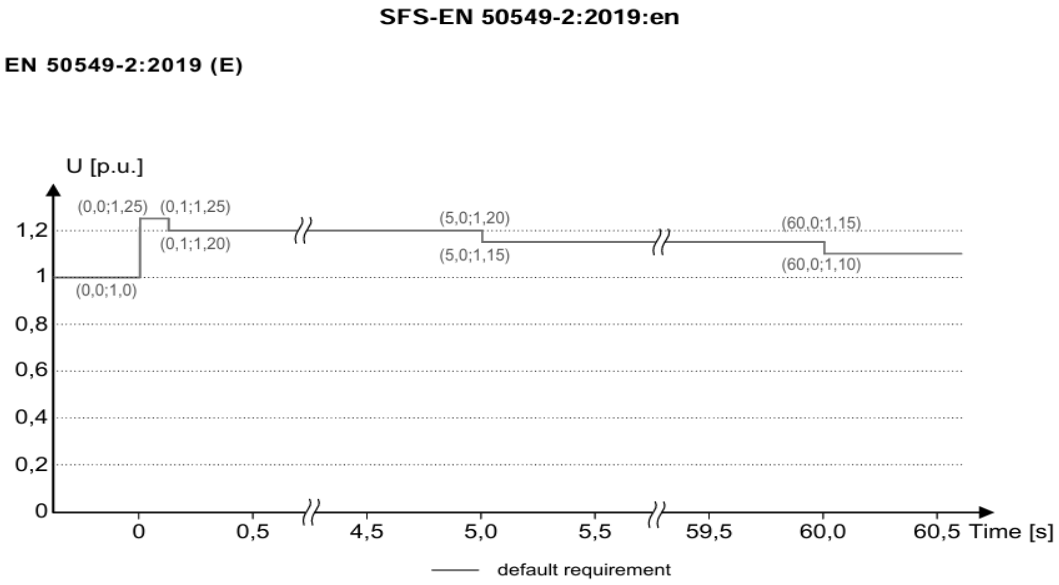


**Figure 4-14**: OVRT Voltage–Time Envelope as Defined in EN 50549-2

Standardized voltage–time profile defining permissible voltage swell magnitudes and durations for which the system must remain connected to the grid.

The system is evaluated based on **(i)** continuous operation during the overvoltage event, **(ii)** compliance with DC-link voltage limits, and **(iii)** stable post-disturbance recovery. The

automated evaluation confirms that all criteria are satisfied, resulting in an overall OVRT pass conditions shown in generated report as follow in **Figure 4-15**

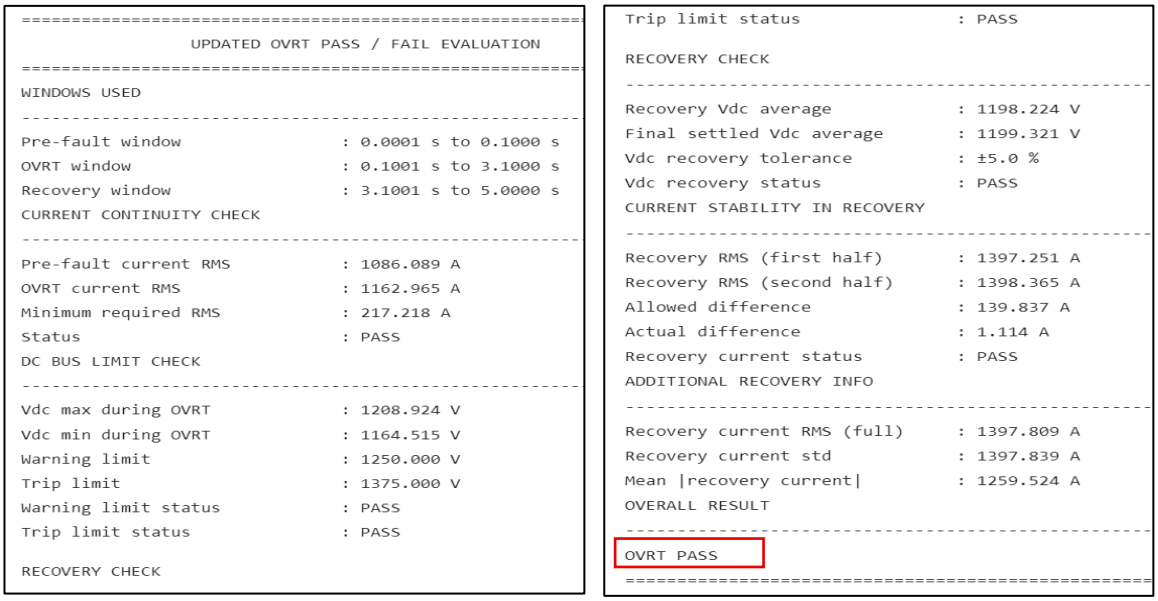

```
============================================================
                UPDATED OVRT PASS / FAIL EVALUATION
============================================================
WINDOWS USED
------------------------------------------------------------
Pre-fault window                : 0.0001 s to 0.1000 s
OVRT window                     : 0.1001 s to 3.1000 s
Recovery window                 : 3.1001 s to 5.0000 s
CURRENT CONTINUITY CHECK
------------------------------------------------------------
Pre-fault current RMS           : 1086.089 A
OVRT current RMS                : 1162.965 A
Minimum required RMS            : 217.218 A
Status                          : PASS
DC BUS LIMIT CHECK
------------------------------------------------------------
Vdc max during OVRT             : 1208.924 V
Vdc min during OVRT             : 1164.515 V
Warning limit                   : 1250.000 V
Trip limit                      : 1375.000 V
Warning limit status            : PASS
Trip limit status               : PASS

RECOVERY CHECK
```

```
Trip limit status               : PASS

RECOVERY CHECK
------------------------------------------------------------
Recovery Vdc average            : 1198.224 V
Final settled Vdc average       : 1199.321 V
Vdc recovery tolerance          : ±5.0 %
Vdc recovery status             : PASS
CURRENT STABILITY IN RECOVERY
------------------------------------------------------------
Recovery RMS (first half)       : 1397.251 A
Recovery RMS (second half)      : 1398.365 A
Allowed difference              : 139.837 A
Actual difference               : 1.114 A
Recovery current status         : PASS
ADDITIONAL RECOVERY INFO
------------------------------------------------------------
Recovery current RMS (full)     : 1397.809 A
Recovery current std            : 1397.839 A
Mean |recovery current|         : 1259.524 A
OVERALL RESULT
------------------------------------------------------------
OVRT PASS
============================================================
```

**Figure 4-15:** OVRT Survivability Assesment Report

Simulation-based verification of DC-link stability, battery voltage validity, continuous operation, and successful recovery, resulting in an overall OVRT pass condition as shown in **Figure 4-15** is taken from post process report.

### 4.10.1 Dynamic Response under Weak Grid

The weak grid condition is selected as the critical case due to its higher sensitivity to converter–grid interaction during voltage disturbances. The AC-side response at the point of common coupling is shown in **Figure 4-16**.

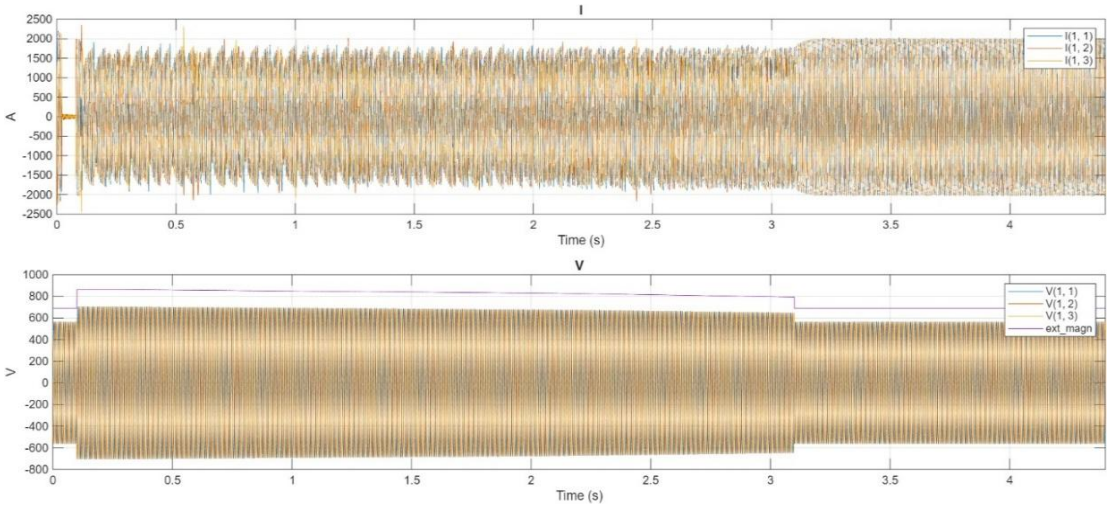


**Figure 4-16**: Three-Phase Voltage and Current at PCC during OVRT (Weak Grid, 3-Level Inverter)

The grid voltage in **Figure 4-16** follows the imposed overvoltage profile, while the current remains continuous and synchronized. Although distortion increases during the swell, no loss of control or disconnection is observed.

The DC-link behavior is illustrated in **Figure 4-17**.

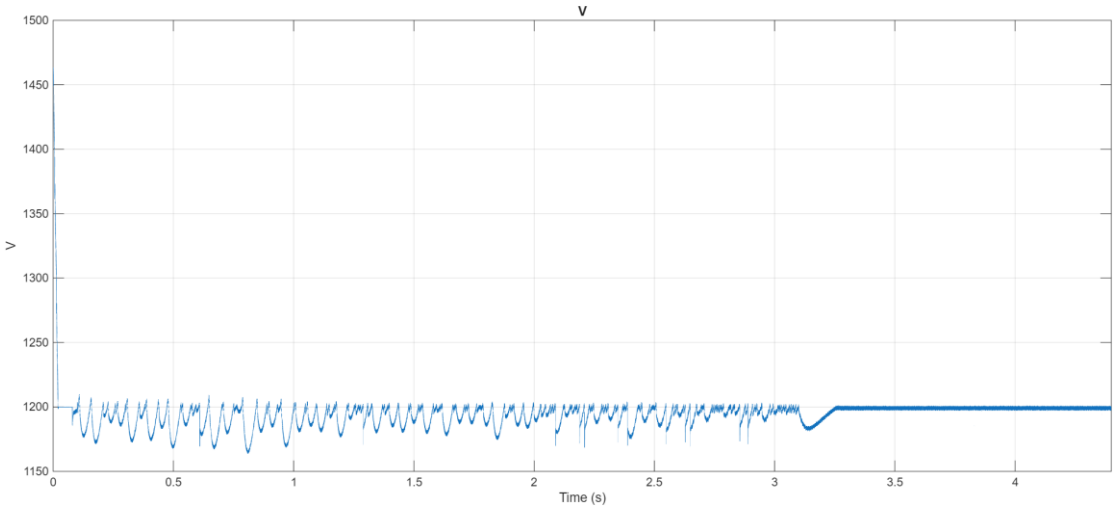


**Figure 4-17**: DC-Link Voltage Response during OVRT (Weak Grid, 3-Level Inverter)

The voltage on the DC bus as shown in **Figure 4-17** is maintained within a range of 1150 V– 1200V during the disturbance event. More importantly, the voltage never exceeds

the maximum allowable limit (1250V) nor approaches the emergency threshold at which a protection relay would act (1375V).

**Below Figure 4-18** and **Figure 4-19** depict the results from the battery side.

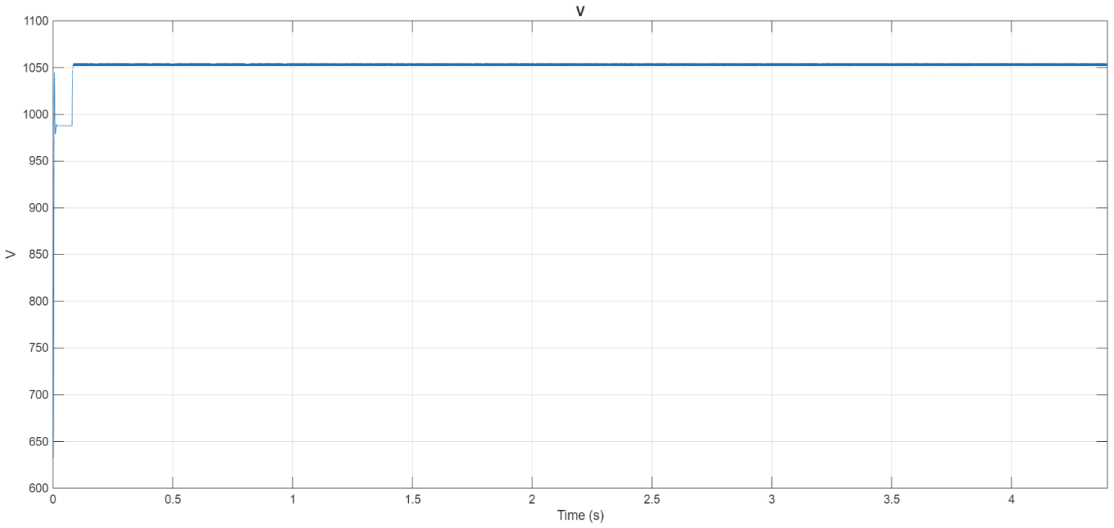


**Figure 4-18**: Battery Terminal Voltage during OVRT

The battery terminal voltage in **Figure 4-18** is not affected due to the rise in grid side voltage level because of effective decoupling using DC-DC converter section and ensuring continuous charging operation.

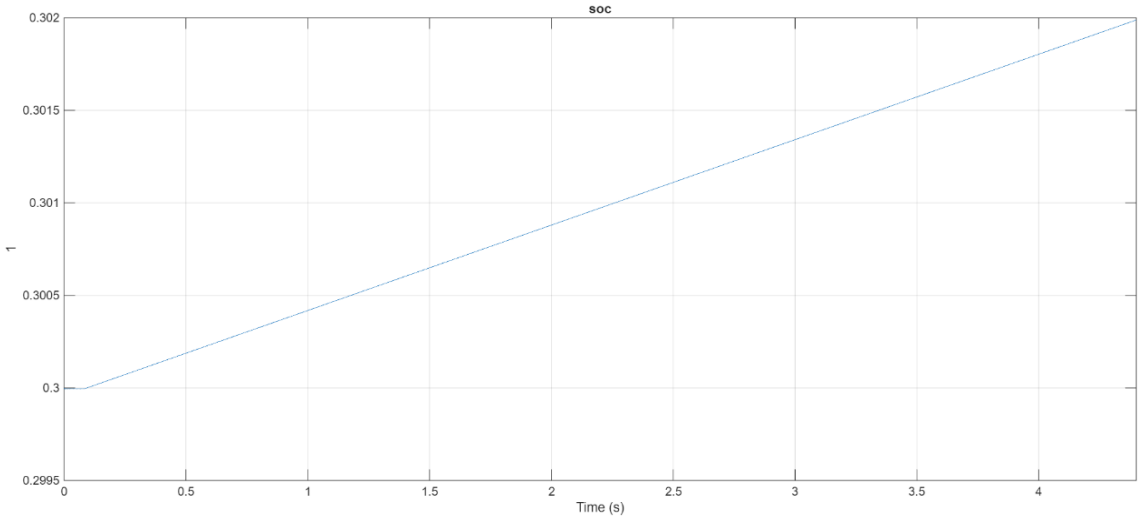


**Figure 4-19**: Evolution of State of Charge (SOC) during OVRT (Weak Grid Case)

The evolution of SOC in **Figure 4-19** during the OVRT experiment shows a consistent charging pattern of the battery without any discontinuities or sudden changes caused by the voltage increase. There are no disruptions in power flow and synchronization between the AFE and DC-DC converter blocks. Therefore, it can be concluded that the battery does not get affected by the grid-side voltage fluctuation during charging.

### 4.10.2 Comparative Performance: 2-Level and 3-Level Inverters

Both inverter topologies are evaluated under identical OVRT conditions to assess their relative performance.

**Table 7**: OVRT Performance Comparison Based on Power Quality Metrics

| Metric | 2-Level | 3-Level | Better |
|---|---|---|---|
| OVRT continuity | Pass | Pass | Both |
| THD(Ia) | 6.397% | 3.096% | 3L |
| Vdc ripple | 2.295% | 3.719% | 2L on this metric |
| Vbat ripple | 0.253% | 0.258% | Nearly same |
| Ibat ripple | 4.092% | 4.161% | Nearly same |

Results of **Table 7** show that both topologies met ride through requirements and stay connected during the fault period. Differences between them become apparent regarding the quality of power:

- 3-level inverter provides smaller grid current THD (~3.1%) than 2-level inverter (~6.4%)
- Both topologies provide an adequate level of DC link voltage ripple. In addition, 2-level inverter is more effective than 3-level inverter in terms of this parameter
- Battery side voltage and current ripples are almost equal for both inverters

It should be noted that despite similar ride through requirements both inverters have significantly different levels of grid current waveforms.

### 4.10.3 Discussion

OVRT results indicate that the design can be operated in the presence of voltage swell without breaking the protection limits for the system. The DC link voltage level does not go near to any critical value; hence, the AFE control scheme efficiently handles the excess energy present in the circuit in the case of over-voltages.

An important point is that the variables on the battery side are not affected at all, which clearly keep on confirming the importance of the DC–DC converter in insulating the battery from the grid. However, the output obtained from the grid current reveals the impact of the inverter topology on its performance during disturbances. The 3-level inverter outperforms the 2-Level one in terms of producing harmonics.

### 4.10.4 Key Observation

OVRT compliance ensures stable operation and protection limit adherence during voltage swells, while the inverter topology primarily influences the quality of the grid current response.

### 4.10.5 Compliance Statement

The designed megawatt charging system meets the OVRT criteria stipulated in EN 50549-2 through:

- remaining connected throughout the voltage swell event
- maintaining DC-link voltage within defined operational and protection limits
- ensuring stable system behavior and controlled recovery

## 4.11 Integrated Discussion

The results gathered from the steady-state operation tests, parametric studies, and grid disturbances give a demonstration of the operating features of charging stations at the

MW level during actual power grid operations. It is important to perform an analysis altogether rather than analyzing each test independently to have a complete grasp of the interrelationship between the grid and the converter system. One of the conclusions that can be drawn from the analysis is the effect of grid stiffness on the converter system. As the short-circuit ratio becomes smaller, grid impedance becomes larger, resulting in higher interactions between the grid and the converter system. This is shown by the rise in harmonic distortion, increased DC-link voltage distortion, and oscillation.

On the other hand, the behavior of the battery side remains relatively invariant under all conditions. In spite of different levels of variation in grid voltage, frequency, and faults, the battery voltage, current, and state-of-charge profiles remain stable and uninterrupted. This proves that the DC-DC conversion stage successfully filters the impact of disturbances on the charging operation. Also, the connection between compliance with the ride-through criterion and the level of power quality is made explicit in the disturbance analysis. Compliance with the ride-through criterion under undervoltage and overvoltage is demonstrated by the ability of the system to maintain its connectivity and recover stability after disturbances. At the same time, higher harmonics and higher ripples have been noticed during the process, especially when operating under weak grids. Thus, ride-through compliance guarantees operational continuity but not power quality.

In the sensitivity analysis of the DC-DC circuit, it becomes clear that the optimization of the parameters through scaling is limited. Switching frequency enhancement can reduce ripple until a certain degree, but beyond that, the increase has little impact. Increased output inductance decreases ripple but is subject to limitations from the battery side standards. Given such constraints, damping turns out to be the best way to eliminate mid-frequencies oscillations and meet IEC ripple requirements.

Converting topology adds yet another dimension of impact on the overall performance. As can be seen from the comparison of two inverter topologies, 2-Level vs. 3-Level, the latter consistently provides better harmonic distortion characteristics. In particular, 3-

level topology is superior in weak grid environment. The cause behind the higher harmonic distortion level of 3-level topology is its inherent ability to synthesize multi-level voltage, reducing the number of harmonics at switching frequency.

Consequently, this means that the use of all three mentioned types of comparison makes it possible to notice that there are several levels of interrelated elements which affect the dynamics of MW charging stations. Hence, the elements which affect the dynamics of MW charging stations can be considered to be the external factors (the state of the network) and internal characteristics of a converter.

# 5 Conclusion and Future Work

This study proves that the stable working of megawatt charger stations can be ensured under different conditions of the electric network by proper designing and controlling of converters. Grid robustness and type of topology become important factors affecting the power quality. This chapter will also touch upon the limitations of the study and future advancements.

## 5.1 Conclusions

The thesis focused on the evaluation of MW-level EV charger systems subjected to actual grid operation using GMVF. As such, the model used for this thesis consists of the AC-DC active front-end converter, DC-DC converter, and the battery charging system operating through a terminal voltage-based CC-CV control strategy. This results in the ability to simulate the dynamic response of the converter as well as its charging capabilities accurately. The findings show that the system attains stable operation under nominal conditions as it maintains megawatt-level power transfer capability. A principal finding is that system performance is strongly influenced by grid conditions at the point of common coupling. For example, the grid weaknesses, defined by low short circuit ratios, are associated with high harmonics, high DC link stresses, and increased coupling between the converter and the grid. On the other hand, the fair grid strengths offer good voltage support and improved power quality.

A comparison of the various types of converter topologies also indicates that the internal design of converters plays an important role in influencing system behavior. In cases where the power grid is highly stable or moderately stable, the 2-level inverter offers sufficient performance, while the 3-level inverter has better performance when the grid is weak. From the above findings, it can be deduced that the selection of a particular converter topology needs to be taken into consideration at the local grid. The system was evaluated under a range of grid operating and disturbance conditions, including ±10%

voltage variation, off-nominal frequency operation, and ride-through events. In all scenarios, the charging system remained operational without any disconnection and maintained controlled charging behavior. These results confirm that the system fulfills the functional intent of grid code requirements by preserving connectivity and ensuring stable recovery during disturbances. From a systems design point of view, it is shown that compliance is not possible only through parameter scaling. Although the switching frequency and the value of the output inductance do affect ripple performance, there are physical limitations on what can be accomplished through this method. In order to reduce mid-frequency ringing and meet IEC standards for ripple performance, damping becomes necessary in the battery side filter.

The findings also confirm that the decoupling of any disturbances from the grid side to the battery side is efficient. The battery voltage, current, and state of charge were stable and uninterrupted during all the test cases, which proves that the DC-to-DC step decouples the charging process from the grid disturbances.

In summary, megawatt EV charging stations can therefore be treated as interactive systems where system performance is determined by the joint effect of grid strength, converter architecture, and control/protection strategies. The developed GMVF-based methodology provides an organized, replicable means of testing such systems in practical grid settings, thereby filling the gap between simulation and implementation of megawatt charging systems.

## 5.2 Key Contributions of the Thesis

This thesis makes the following key contributions to the analysis and design of megawatt-scale electric vehicle charging systems:

**1. Development of Grid-Integrated MCS Validation Framework (GMVF) for Megawatt-Charging-Systems**

A simulation-based methodology was formulated for assessing the performance of

megawatt-scale electric vehicle chargers against practical electrical grid requirements. The methodology includes the inclusion of models for converters (active front end and isolated DC–DC converter), battery charging behavior based on voltage-dependent CC–CV charge control method, and a set of operating scenarios for electrical grids. It helps us to have a reproducible methodology for assessing grid compliance without full-scale hardware deployment.

**2. Quantification of Grid Strength Impact on System Performance**

Grid strength, measured using the short circuit ratio (SCR), is found to be the main external influence on system dynamics. It is clear from the findings that under weak-grid conditions, harmonic distortion levels are higher, DC-link voltage stress increases, and grid-interaction effects become more pronounced compared to strong grids. The need to conduct studies on the grid-connected side i.e. PCC of the charging system, becomes evident from these findings.

**3. Comparative Evaluation of Converter Topologies with Grid-Dependent Design Insight**

The comparative analysis between the 2-level, and 3-level inverter types has been made in varying grid strengths. From the analysis, although the 2-level type converters offer sufficient performance in strong grids, the 3-level converters exhibit superior performance in terms of harmonics as well as stability in weak grids. Hence, the topology of the converter needs to be chosen depending on grid strength.

**4. Validation of System Operation under Grid Operating and Disturbance Conditions**

The proposed method was tested through different scenarios of operating conditions such as ±10% voltage fluctuation, off-frequency operations, and ride-through conditions (low voltage ride-through [LVRT] and overvoltage ride-through [OVRT]). It is found that the proposed system works continuously and recovered successfully without any failure in achieving its objective according to grid code requirements.

**5. Identification of Damping as a Critical Design Requirement for IEC-Compliant Ripple Performance**

From sensitivity analysis of the DC-to-DC converter, it is clear that increasing the switching frequency and inductance values cannot satisfy the ripple criteria according to IEC standards because of intrinsic constraints. The only parameter left, which can meet the specified criteria, is battery-side filter damping, other than controller tweaks.

**6. Demonstration of Effective Decoupling between Grid-Side Disturbances and Battery-Side Operation**

In all tested cases, even under poor grid and disturbance conditions, the battery's voltage, current, and SOC remain stable and continuous. Thus, the effectiveness of decoupling the charging process through the use of DC-DC conversion can be confirmed without any doubt.

## 5.3 Limitations of The Study

While this thesis provides a comprehensive simulation-based evaluation of megawatt-scale EV charging systems, certain limitations must be acknowledged.

First, the current research uses simulation experiments developed on MATLAB/Simulink software. Although the mathematical model takes into account converter dynamics and real control approaches, experimental validation is not provided in the study. Therefore, it is impossible to include practical issues such as measurement error, data transmission delays, and heat generation into the analysis (Freijedo et al., 2011; Jayawardana et al., 2022).

Second, grid interaction is modeled using equivalent models based on the short-circuit ratio and X/R ratio. While such modeling techniques are useful in analyzing strong, medium, and weak grids, they do not adequately account for all the dynamic interactions of distribution grids, especially those which are unbalanced, have harmonics, or are asymmetrical (Huang et al., 2021; Blaabjerg et al., 2006).

Third, the control method chosen for this study uses a grid following control scheme. Although this is consistent with present practices in industry with regards to charging of electric vehicles, other methods such as grid forming control or virtual synchronous machine control were not considered. Such methods would improve system operation under poor grid conditions and could be seen as an extension of this research (Zhong & Weiss, 2011; Rocabert et al., 2012).

Fourth, the battery model is based on an electrical equivalent representation using SOC-dependent open-circuit voltage and internal resistance. Although this approach captures the dominant electrical behavior required for charging control, it does not include detailed electrochemical dynamics, aging effects, or temperature dependence (Plett, 2004).

This research makes use of the traditional SRF-PLL to perform grid synchronization; the effect of advanced PLLs such as DSOGI or adaptive technique, for weak-grid situations has not been examined (Karimi-Ghartemani, 2014).

Lastly, the effects related to EMC, such as the parasitic capacitances of transformers and noise coupling due to switching phenomena, are not modeled explicitly. Even though the output is modeled considering damping and filtering, EMC effects would have needed modeling on a finer level (Bollen, 2000).

Despite these limitations, the developed framework captures the key dynamics governing megawatt charging system performance and provides a reliable basis for comparative analysis and design-oriented evaluation under realistic grid conditions.

## 5.4 Future Work

The findings of the thesis suggest multiple paths for future research to develop MW-class EV fast-charging stations. It seems logical that the GMVF approach proposed above could be experimentally validated via HIL or prototype-level testing to verify simulation

results on real systems (Freijedo et al., 2011; Jayawardana et al., 2022). This would allow consideration of actual system features, such as noise measurement, control delays, and other non-idealities. Research on the implementation of more sophisticated control schemes, especially the application of grid-forming control techniques like the virtual synchronous machine (VSM) control scheme, may enhance the system's performance when dealing with weak-grid scenarios (Zhong & Weiss, 2011; Rocabert et al., 2012). Further research can be extended to cover multi-charger systems and charging stations, where the impact of the interactions among several high-power converters needs to be considered from the point of common coupling standpoint (Althurthi & Rajashekara, 2025). Integration of battery energy storage systems (BESS) at the DC-link level represents another promising direction, enabling enhanced grid support, peak shaving, and improved operational flexibility (Tu et al., 2019).

The future research could also focus on dynamic adjustment of the converter characteristics during power grid faults using adaptive LVRT techniques. This method will help stabilize the DC link and achieve better transient responses during voltage sags (ENTSO-E, 2016). Exploring more sophisticated synchronization methods, including DSOGI-PLL and adaptive PLL approaches, to achieve better system operation under weak grid conditions and better DC link stability during disturbances could also be possible (Karimi-Ghartemani, 2014).

Finally, bidirectional power flow capability (vehicle-to-grid, V2G) can be considered as an important extension of this work. Although this capability is still in the works, with plans to integrate it into future iterations of IEC 61851-23-3, its inclusion will present further difficulties in control design, protective device coordination, and grid support functions. Extending the present framework to support bidirectional operation would enable a comprehensive evaluation of grid-interactive charging systems in future power systems (Kempton & Tomic, 2005).

## References

Acharige, S. S. G., Haque, M. E., Arif, M. T., Hosseinzadeh, N., Hasan, K. N., & Oo, A. M. T. (2023). Review of electric vehicle charging technologies, standards, architectures, and converter configurations. IEEE Access, 11, 41218–41255. https://doi.org/10.1109/ACCESS.2023.3267164

Althurthi, S. B., & Rajashekara, K. (2025). An optimal multi-zone fast-charging system architecture for MW-scale EV charging sites. *World Electric Vehicle Journal, 16*(7). https://doi.org/10.3390/wevj16070389

Blaabjerg, F., Teodorescu, R., Liserre, M., & Timbus, A. V. (2006). Overview of control and grid synchronization for distributed power generation systems. IEEE Transactions on Industrial Electronics, 53(5), 1398–1409. https://doi.org/10.1109/TIE.2006.881997

Bollen, M. H. J. (2000). *Understanding power quality problems: Voltage sags and interruptions*. IEEE Press. https://ieeexplore.ieee.org/servlet/opac?bknumber=5270869

CENELEC. (2019). *EN 50549-2: Requirements for generating plants to be connected in parallel with distribution networks – Part 2: Connection to medium-voltage networks*.

Celanovic, N., & Boroyevich, D. (2000). *A comprehensive study of neutral-point voltage balancing problem in three-level neutral-point-clamped voltage source PWM inverters*. *IEEE Transactions on Power Electronics, 15*(2), 242–249. https://doi.org/10.1109/63.838096

Das, H. S., Rahman, M. M., Li, S., & Tan, C. W. (2020). *Electric vehicles standards, charging infrastructure, and impact on grid integration: A technological review*. Renewable and Sustainable Energy Reviews, 120, 109618. https://doi.org/10.1016/j.rser.2019.109618

ENTSO-E. (2016). *Requirements for generators (RfG) and fault ride-through capabilities*. European Network of Transmission System Operators for Electricity. Annual Report: What did ENTSO-E do in 2016?

ENTSO-E. (2023). *Impact of electric vehicles on the power system*. European Network of Transmission System Operators for Electricity. Position paper on "Deployment of Heavy-Duty Electric Vehicles and their Impact on the Power System"

Freijedo, F. D., et al. (2011). Tuning of phase-locked loops for power converters under distorted utility conditions. *IEEE Transactions on Industrial Electronics*. https://doi.org/10.1109/TIA.2009.2031790

Habib, S., Khan, M. M., Abbas, F., Sang, L., Shahid, M. U., & Tang, H. (2018). A comprehensive study of implemented international standards, technical challenges, impacts and prospects for electric vehicles. *IEEE Access, 6*, 13866–13890. https://doi.org/10.1109/ACCESS.2018.2812303

Huang, L., Wang, X., Blaabjerg, F., & Loh, P. C. (2020). Grid-synchronization stability analysis and loop shaping for PLL-based power converters with different reactive power control. *IEEE Transactions on Smart Grid, 11*(1), 501–516. https://doi.org/10.1109/TSG.2019.2924295

IEC. (2024). *IEC 61851-23-3: Electric vehicle conductive charging system – Part 23-3: DC EV supply equipment for megawatt charging systems* (Draft standard).

IEEE Standards Association. (2020). *IEEE Std 519-2020: Recommended practice and requirements for harmonic control in electric power systems*. 10.1109/IEEESTD.2022.9848440

International Energy Agency. (2025). *Global EV outlook 2025: Trends in electric mobility*. IEA. https://www.iea.org/reports/global-ev-outlook-2025

Karimi-Ghartemani, M. (2014). Enhanced phase-locked loop structures for power and energy applications. *IEEE Transactions on Power Electronics, 29*(8), 3919–3929. https://ieeexplore.ieee.org/servlet/opac?bknumber=6798067

Karimi-Ghartemani, M. (2014). Enhanced phase-locked loop. *IEEE Transactions on Power Electronics, 29*(8), 3919–3929. https://doi.org/10.1002/9781118795187.ch2

Kempton, W., & Tomic, J. (2005). Vehicle-to-grid power fundamentals: Calculating capacity and net revenue. *Journal of Power Sources, 144*(1), 268–279. https://doi.org/10.1016/j.jpowsour.2004.12.025

Mohamed, A. A. S., et al. (2023). Hierarchical control of megawatt-scale charging stations for electric trucks with distributed energy resources. *IEEE Transactions on Transportation Electrification, 9*(4), 4951–4963. https://doi.org/10.1109/TTE.2022.3167647

Liserre, F., Teodorescu, R., & Blaabjerg, F. (2006). Stability of photovoltaic and wind turbine grid-connected inverters for a large set of grid impedance values. *IEEE Transactions on Power Electronics, 21*(1), 263–272. https://doi.org/10.1109/TPEL.2005.861185

Mercedes-Benz Trucks. (2024). *eActros 600 – Technical specifications*. https://www.mercedes-benz-trucks.com

Jayawardana, I., Ho, C. N. M., & Zhang, Y. (2022). A comprehensive study and validation of a power-HIL testbed for evaluating grid-connected EV chargers. *IEEE Journal of Emerging and Selected Topics in Power Electronics, 10*(2), 2395–2410. https://doi.org/10.1109/JESTPE.2021.3093303

Moorthy, R. S. K., et al. (2024). *Megawatt scale charging system architecture*. Oak Ridge National Laboratory. Megawatt Scale Charging System Architecture - Oak Ridge National Laboratory

Nikitha, L., Anil, L., Tripathi, A., & Nagesh, S. (2017). Effect of electrical vehicle charging on power quality. In *2017 International Conference on Circuit, Power and Computing Technologies (ICCPCT)*. IEEE. https://doi.org/10.1109/ICCPCT.2017.8074344

Plett, G. L. (2004). *Extended Kalman filtering for battery management systems of LiPB-based HEV battery packs: Part 3. State and parameter estimation*. *Journal of Power Sources, 134*(2), 277–292. https://doi.org/10.1016/j.jpowsour.2004.02.033

Rocabert, J., Luna, A., Blaabjerg, F., & Rodriguez, P. (2012). Control of power converters in AC microgrids. *IEEE Transactions on Power Electronics, 27*(11), 4734–4749. https://doi.org/10.1109/TPEL.2012.2199334

Rodríguez, J., Lai, J. S., & Peng, F. Z. (2002). Multilevel inverters: A survey of topologies, controls, and applications. *IEEE Transactions on Industrial Electronics, 49*(4), 724–738. https://doi.org/10.1109/TIE.2002.801052

Scania Group. (2024). *Battery electric trucks – Range and performance data*. https://www.scania.com

Tesla Inc. (2023). *Tesla Semi – Product overview*. https://www.tesla.com/semi

Texas Instruments. (2021). *Design considerations for high-power EV charging systems* (Application Report). Comparison of AC/DC Power-Conversion Topologies for Three-Phase Industrial Systems

Texas Instruments. (2021). *Design considerations for high-power EV charging systems* (Application Report). https://www.ti.com

Tu, H., Feng, H., Srdic, S., & Lukic, S. (2019). Extreme fast charging of electric vehicles: A technology overview. *IEEE Transactions on Transportation Electrification, 5*(4), 861–878. https://doi.org/10.1109/TTE.2019.2958709

Volvo Trucks. (2024). *Volvo FH Aero Electric – Product specifications*. https://www.volvotrucks.com

Wang, S., Crosier, R., & Chu, Y. (2012). Investigating the power architectures and circuit topologies for megawatt superfast electric vehicle charging stations with enhanced grid support functionality. In *2012 IEEE International Electric Vehicle Conference (IEVC)* (pp. 1–8). IEEE. https://doi.org/10.1109/IEVC.2012.6183177

Zhong, Q.-C., & Weiss, G. (2011). Synchronverters: Inverters that mimic synchronous generators. *IEEE Transactions on Industrial Electronics, 58*(4), 1259–1267. https://doi.org/10.1109/TIE.2010.2048839

Zhu, X., Mather, B., & Mishra, P. (2020). Grid impact analysis of heavy-duty electric vehicle charging stations. In *2020 IEEE Power & Energy Society Innovative Smart Grid Technologies Conference (ISGT)* (pp. 1–5). IEEE. https://doi.org/10.1109/ISGT45199.2020.9087651

# Appendices

## Appendix A — System Parameters

This appendix summarizes the key parameters used in the simulation model. Derived control parameters and intermediate variables are omitted for clarity, while all primary system parameters required for reproducibility are included

### A.1 Grid and Point of Common Coupling (PCC)

| Parameter | Symbol | Value | Unit | Description |
|---|---|---|---|---|
| Line-to-line voltage | $V_{LL}$ | 690 | V | Nominal grid voltage |
| System frequency | $f$ | 50 | Hz | Grid frequency |
| Grid condition (weak grid case) | SCR | 3 | – | Short-circuit ratio |
| X/R ratio | X/R | 10 | – | Grid impedance ratio |
| Line inductance | $L_{grid}$ | 2.10e-4 | H | Grid-side inductance |
| Line resistance | $R_{grid}$ | 6.60e-3 | Ω | Grid-side resistance |

### A.2 AC–DC Converter (Active Front-End)

| Parameter | Symbol | Value | Unit | Description |
|---|---|---|---|---|
| DC-link voltage | $V_{dc}$ | 1200 | V | Rated DC output voltage |
| DC current | $I_{dc}$ | 2000 | A | Rated DC current |
| Switching frequency | $f_{sw,AFE}$ | 10 kHz | Hz | Converter switching frequency |
| Output capacitance | $C_{out}$ | 15 mF | F | Output capacitor |

| | | | | |
|---|---|---|---|---|
| Maximum AC current | – | ±3000 | A | Converter current limits |
| Minimum DC voltage | – | 600 | V | Operational lower limit |

## A.3 DC-Link Parameters

| Parameter | Symbol | Value | Unit | Description |
|---|---|---|---|---|
| DC-link voltage | $V_{dc}$ | 1200 | V | Nominal DC-link voltage |
| DC-link capacitance | $C_{dc}$ | 120 mF | F | Energy buffering element |

## A.4 DC–DC Converter

| Parameter | Symbol | Value | Unit | Description |
|---|---|---|---|---|
| Switching frequency | $f_{sw,DC}$ | 40 kHz | Hz | DC–DC switching frequency |
| Converter inductance | $L_{dc}$ | 25 µH | H | Primary inductance |
| Transformer magnetizing inductance | $L_m$ | 2 | H | Transformer magnetization |
| Transformer winding factor | – | 0.90 | – | Efficiency/turns factor |
| Controller gain (proportional) | $K_p$ | 4 | – | Current control |
| Controller gain (integral) | $K_i$ | 2 | – | Current control |

## A.5 Battery System

| Parameter | Symbol | Value | Unit | Description |
|---|---|---|---|---|
| Battery nominal voltage | $V_{bat}$ | ~1000 | V | Pack nominal voltage |

| | | | | |
|---|---|---|---|---|
| Battery full-charge voltage | – | ~1168 | V | Load Side |
| Terminal Full Charge Voltage | | ~1205 | V | Load Side actual voltage |
| Rated current | $I_{bat}$ | 1200 | A | Charging current |
| Capacity | $C_{bat}$ | 727.51 | Ah | Battery capacity |
| Inductance | $L_{bat}$ | 99 µH | H | Output filter inductance |
| Output capacitance | $C_{out}$ | 15 mF | F | Battery-side capacitor |
| Damping resistor | $R_d$ | 0.027 | Ω | Damping element |
| Initial SOC | – | 0.30 | – | Initial state of charge |
| Cells in series | – | 278 | – | Voltage scaling |
| Parallel strings | – | 266 | – | Capacity scaling |
| Single Cell Capacity | | 2.735Ah | | Cell Scaling |

## A.6 Simulation Parameters

| **Parameter** | **Symbol** | **Value** | **Unit** | **Description** |
|---|---|---|---|---|
| Simulation cycles | – | 40 | cycles | Number of AC cycles |
| Simulation time | $T_{sim}$ | 0.8 | s | Total simulation duration |
| Sampling time | $T_s$ | 1e-5 | s | Controller sampling time |

## A.7 Converter Variants

| Configuration | Description |
|---|---|
| Average model | Simplified converter representation |
| Two-Level (2L) | Conventional inverter topology |
| Three-Level (3L) | NPC-based multilevel inverter |

## A.8 DC Link Energy Buffering Time

For $C_{dc} = 120\,mF = 0.12\,F$ and $V_{dc} = 1200\,V$:

$$E_{dc} = \frac{1}{2} \times 0.12 \times 1200^2 = 86.4\,kJ$$

At rated DC-side power:

$$P = V_{dc} I_{dc} = 1200 \times 2000 = 2.4\,MW$$

$$t = \frac{E_{dc}}{P} = \frac{86.4\,kJ}{2.4\,MW} = 0.036\,s \approx 36\,ms$$

## A.9 Simulation Solver Configuration

| Parameter | Setting |
|---|---|
| Solver type | Variable-step |
| Solver | daessc (Simscape) |
| Max step size | 5e-5 s |
| Relative tolerance | 1,00E-03 |
| Absolute tolerance | 1,00E-05 |
| Local solver | Enabled |
| Local solver type | Backward Euler |
| Local sample time | 2e-5 s |

## Appendix B — IEC-Based Battery Current Ripple Evaluation

| Configuration | 10 Hz Band | 5 kHz Band | 150 kHz Band |
|---|---|---|---|
| Average – Strong | PASS | FAIL | PASS |
| Average – Moderate | PASS | FAIL | PASS |
| Average – Weak | PASS | FAIL | PASS |
| 2-Level – Strong | PASS | FAIL | PASS |
| 2-Level – Moderate | PASS | FAIL | PASS |
| 2-Level – Weak | PASS | FAIL | PASS |
| 3-Level – Strong | PASS | FAIL | PASS |
| 3-Level – Moderate | PASS | FAIL | PASS |
| 3-Level – Weak | PASS | FAIL | PASS |

It can be concluded that all configurations exceed the IEC limit in the 5 kHz band, indicating that additional filtering or damping is required to achieve full compliance.

## Appendix C — IEC-Based Battery Current Ripple Evaluation after Sensitivity Analysis

| Configuration | 10 Hz Band | 5 kHz Band | 150 kHz Band |
|---|---|---|---|
| Average – Strong | PASS | PASS | PASS |
| Average – Moderate | PASS | PASS | PASS |
| Average – Weak | PASS | PASS | PASS |
| 2-Level – Strong | PASS | PASS | PASS |
| 2-Level – Moderate | PASS | PASS | PASS |
| 2-Level – Weak | PASS | PASS | PASS |
| 3-Level – Strong | PASS | PASS | PASS |
| 3-Level – Moderate | PASS | PASS | PASS |
| 3-Level – Weak | PASS | PASS | PASS |

# Appendix D — THD vs DC Bus Rating (2000 A Vs 1500A)

## D.1 — Average Model Performance (THD vs Current Rating)

| Grid Condition | Current (A) | Power (MW) | THD (%) | Vdc Ripple (%) | Ibat Ripple (%) | Vbat Ripple (%) |
|---|---|---|---|---|---|---|
| Strong Grid | 2000 | 2.4 | 0.227 | 0.054 | 0.721 | 0.044 |
| Moderate Grid | 2000 | 2.4 | 2.967 | 0.217 | 0.726 | 0.045 |
| Weak Grid | 2000 | 2.4 | 6.868 | 0.518 | 0.722 | 0.044 |
| Strong Grid | 1500 | 1.8 | 0.250 | 0.054 | 0.725 | 0.045 |
| Moderate Grid | 1500 | 1.8 | 1.697 | 0.217 | 0.728 | 0.045 |
| Weak Grid | 1500 | 1.8 | 7.264 | 0.518 | 0.725 | 0.045 |

## D.2 — 2-Level Inverter Performance (THD vs Current Rating)

| Grid Condition | Current (A) | Power (MW) | THD (%) | Vdc Ripple (%) | Ibat Ripple (%) | Vbat Ripple (%) |
|---|---|---|---|---|---|---|
| Strong Grid | 2000 | 2.4 | 2.254 | 0.117 | 0.720 | 0.044 |
| Moderate Grid | 2000 | 2.4 | 3.806 | 0.255 | 0.721 | 0.044 |
| Weak Grid | 2000 | 2.4 | 2.582 | 0.525 | 0.720 | 0.044 |
| Strong Grid | 1500 | 1.8 | 2.299 | 0.1218 | 0.7306 | 0.248* |
| Moderate Grid | 1500 | 1.8 | 2.783 | 0.259 | 0.728 | 0.045 |
| Weak Grid | 1500 | 1.8 | 3.177 | 0.525 | 0.722 | 0.044 |

## D.3 — 3-Level Inverter Performance (THD vs Current Rating)

| Grid Condition | Current (A) | Power (MW) | THD (%) | Vdc Ripple (%) | Ibat Ripple (%) | Vbat Ripple (%) |
|---|---|---|---|---|---|---|
| Strong Grid | 2000 | 2.4 | 1.843 | 0.094 | 0.725 | 0.045 |
| Moderate Grid | 2000 | 2.4 | 4.164 | 0.232 | 0.722 | 0.044 |
| Weak Grid | 2000 | 2.4 | 5.834 | 0.468 | 0.720 | 0.044 |
| Strong Grid | 1500 | 1.8 | 1.581 | 0.108 | 0.729 | 0.045 |
| Moderate Grid | 1500 | 1.8 | 3.047 | 0.2318 | 0.728 | 0.0448 |
| Weak Grid | 1500 | 1.8 | 2.577 | 0.525 | 0.728 | 0.045 |

## Appendix E — DC Bus Link Capacitance

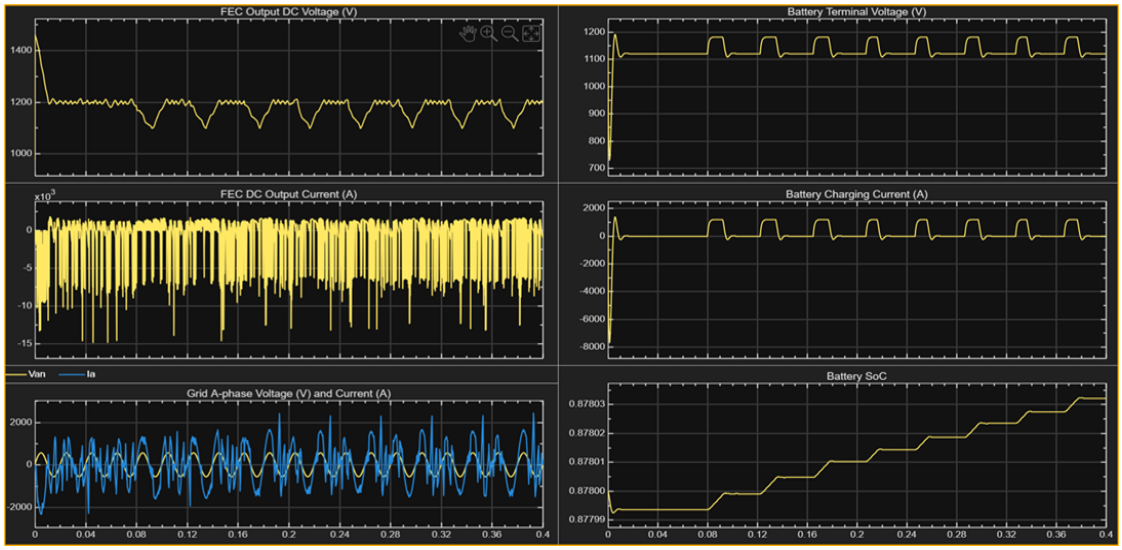


**Figure 5-1**: System Response for Moderate Grid at reduced DC Link by 33.33% for 3 Level Inverter

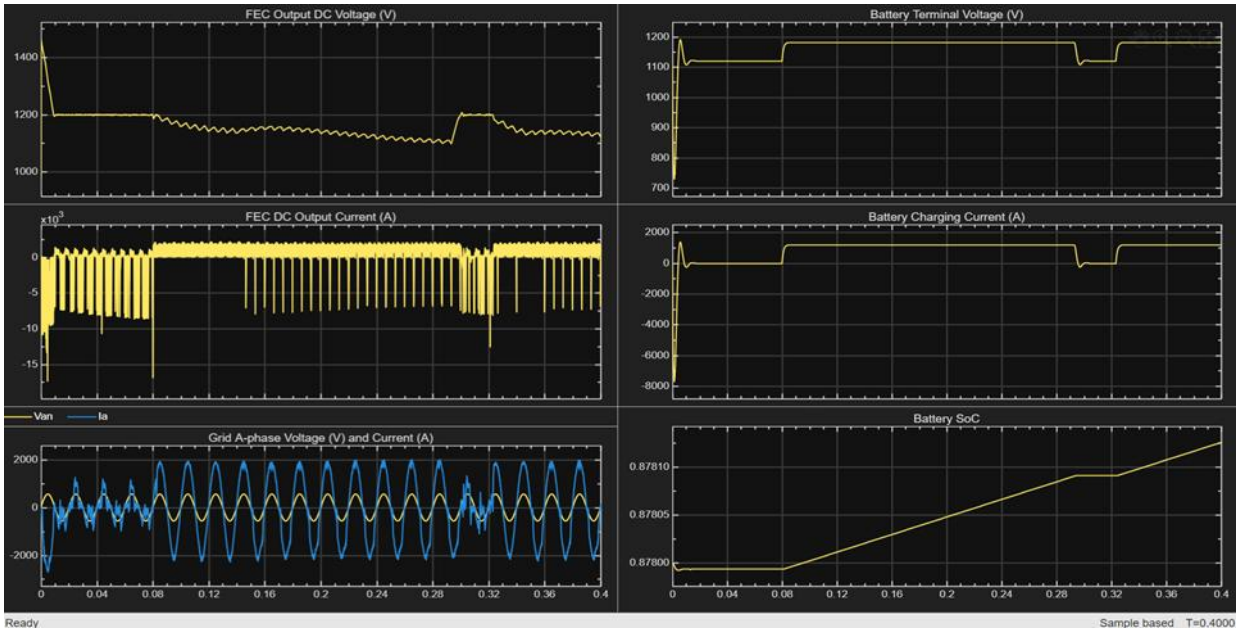


**Figure 5-2**: Reduced DC Link capacitance for Strong Grid by 33.33% for 3 Level Inverter

## Appendix F — CC-CV Full algoritm

```
function Iref = CCCV_Supervisor(Vbat, SOC, Vcv_ref, Icc_ref)
%#codegen
% CC-CV supervisor with AND condition:
% Enter CV only if:
%   1) Vbat >= Vcv_ref
%   2) SOC  >= 87.9%
%
% Output:
%   Iref -> current reference for inner DC-DC current con-
troller

%% ---------------- Tunables ----------------
Ts            = 1e-5;         % controller sample time [s]
[1/(10*rectifier.SwitchFrequency)]
SOC_th    = 0.879;      % SOC threshold for CV entry
SOC_hys   = 0.01;      % SOC hysteresis
V_hys     = 5.0;       % voltage hysteresis [V]

% CV taper PI gains (start gentle)
Kp_cv     = 0.4;
Ki_cv     = 15.0;

% Minimum current at end of charge
I_min_frac = 0.005;     % 0.5% of rated current

% Slew-rate limiting for smooth current transition
```

```
slew_Aps  = 50;       % A/s (reduce more if taper is still
too fast)

%% ---------------- Derived ----------------
I_min  = I_min_frac * Icc_ref;
dI_max = slew_Aps * Ts;

%% ---------------- Persistents ----------------
persistent mode int_v Iprev
if isempty(mode),  mode  = false; end   % false=CC, true=CV
if isempty(int_v), int_v = 0.0;   end
if isempty(Iprev), Iprev = Icc_ref; end

%% ---------------- Mode Logic ----------------
% Enter CV only when BOTH conditions are true
if ~mode
    if (Vbat >= Vcv_ref) && (SOC >= SOC_th)
        mode = true;
    end
else
    % Exit CV only if either variable falls back enough
    if (Vbat <= (Vcv_ref - V_hys)) || (SOC <= (SOC_th -
SOC_hys))
        mode = false;
    end
end

%% ---------------- Reference Generation ----------------
if ~mode
    % CC mode
    Icmd = Icc_ref;
    int_v = 0.0;    % reset integrator for clean CV entry
later
else
    % CV mode
    ev = Vcv_ref - Vbat;

    % Integrator
    int_v = int_v + ev * Ts;

    % PI-generated taper current
    Icmd = Kp_cv * ev + Ki_cv * int_v;

    % Limit to [I_min, Icc_ref]
    if Icmd > Icc_ref
        Icmd = Icc_ref;
    elseif Icmd < I_min
        Icmd = I_min;
    end
end

%% ---------------- Slew Rate Limiter ----------------
dI = Icmd - Iprev;
```

```
if dI > dI_max
    Iref = Iprev + dI_max;
elseif dI < -dI_max
    Iref = Iprev - dI_max;
else
    Iref = Icmd;
end

Iprev = Iref;
```

## Appendix G — Protection and Supervision Algorithm

```
function [switch_cmd, gate_en, Iref_out, fault_latched, sta-
tus] = ...
    MCS_Protection_Supervisor(enable_cmd, Vdc, Vbat, Ibat,
Iref_in)
%#codegen
%
% Fully updated MCS Protection Supervisor
%
% Features:
% - NO manual reset input required
% - automatic startup blanking at beginning of simulation
% - DC bus stabilization delay before connection
% - post-connect blanking time to ignore intentional connec-
tion transient
% - normal side-B voltage limit = 1250 V
% - emergency shutdown threshold = 1375 V
% - int32-safe counters for MATLAB Function block code gen-
eration
%
% Inputs:
%   enable_cmd   : main charging enable (0/1)
%   Vdc          : DC bus voltage [V]
%   Vbat         : battery terminal voltage [V]
%    Ibat           : battery current [A] (positive during
charging)
%   Iref_in     : current reference from CCCV supervisor [A]
%
% Outputs:
%   switch_cmd     : 0=open, 1=close
%   gate_en        : 0=disable PWM, 1=enable PWM
%   Iref_out       : protected current reference [A]
%   fault_latched  : latched fault flag
%   status         : status code
%
% Status:
%   0 = idle
%   1 = waiting for DC bus stabilization
%   2 = normal charging
%   3 = controlled shutdown in progress
```

```
%   4 = emergency shutdown / fault latched
%   5 = post-connect blanking active
%   6 = startup blanking active

%% ================ Tunable parameters ================
Ts = 1e-5;    % controller sample time [s]

% -------- Side B voltage logic (MCS) --------
Vbat_max_normal      = 1250.0;   % normal maximum negotiated
side-B voltage [V]
Vbat_emergency_trip  = 1375.0;   % emergency shutdown thresh-
old [V]

% -------- DC bus protection --------
Vdc_min_connect       = 1100.0;    % minimum DC bus voltage
before closing switch [V]
Vdc_max_warn          = 1250.0;    % start limiting / warning
region [V]
Vdc_emergency_trip    = 1375.0;    % hard trip threshold [V]

% -------- Current protection --------
Ibat_max_limit       = 1400.0;    % charging overcurrent trip
[A]

% -------- Timing --------
t_startup_blank      = 0.05;      % ignore all faults during
initial startup [s]
t_bus_stable        = 0.03;      % wait before closing switch
[s]
t_post_connect_blank = 0.03;      % ignore normal faults after
closing switch [s]
t_fault_debounce     = 0.003;     % normal fault debounce [s]
t_emergency_debounce = 0.001;     % emergency fault debounce
[s]

% -------- Safe shutdown --------
ramp_down_Aps        = 5e4;       % ramp current down during
controlled shutdown [A/s]
I_open_thresh         = 20.0;      % open switch only when
current below this [A]

%% ================ Derived ================
N_startup     = int32(max(1, round(t_startup_blank       /
Ts)));
N_bus_stable  = int32(max(1, round(t_bus_stable          /
Ts)));
N_blank        = int32(max(1, round(t_post_connect_blank /
Ts)));
N_fault       = int32(max(1, round(t_fault_debounce      /
Ts)));
N_emg          = int32(max(1, round(t_emergency_debounce /
Ts)));
dI_down      = ramp_down_Aps * Ts;
```

```
%% ================ Persistent states ================
persistent startup_cnt bus_cnt blank_cnt ovdc_cnt ovbat_cnt
ocbat_cnt emg_cnt
persistent fault_lat shutdown_mode emg_mode
persistent iref_state sw_state gate_state sw_prev

if isempty(startup_cnt),    startup_cnt = int32(0); end
if isempty(bus_cnt),        bus_cnt = int32(0); end
if isempty(blank_cnt),      blank_cnt = int32(0); end
if isempty(ovdc_cnt),       ovdc_cnt = int32(0); end
if isempty(ovbat_cnt),      ovbat_cnt = int32(0); end
if isempty(ocbat_cnt),      ocbat_cnt = int32(0); end
if isempty(emg_cnt),        emg_cnt = int32(0); end
if isempty(fault_lat),      fault_lat = false; end
if isempty(shutdown_mode),  shutdown_mode = false; end
if isempty(emg_mode),       emg_mode = false; end
if isempty(iref_state),     iref_state = 0.0; end
if isempty(sw_state),       sw_state = false; end
if isempty(gate_state),     gate_state = false; end
if isempty(sw_prev),        sw_prev = false; end

%%    =================    Automatic    startup    blanking
=================
startup_active = false;
if startup_cnt < N_startup
    startup_cnt = startup_cnt + int32(1);
    startup_active = true;

    % Automatically clear everything during startup
    fault_lat = false;
    shutdown_mode = false;
    emg_mode = false;

    bus_cnt = int32(0);
    blank_cnt = int32(0);
    ovdc_cnt = int32(0);
    ovbat_cnt = int32(0);
    ocbat_cnt = int32(0);
    emg_cnt = int32(0);

    iref_state = 0.0;
    sw_state = false;
    gate_state = false;
end

%% ================ Emergency detection ================
% Emergency protection is disabled only during startup blank-
ing
if ~startup_active
    if (Vbat >= Vbat_emergency_trip) || (Vdc >= Vdc_emer-
gency_trip)
        emg_cnt = emg_cnt + int32(1);
```

```
    else
        emg_cnt = int32(0);
    end

    if emg_cnt >= N_emg
        emg_mode = true;
        fault_lat = true;
    end
end

%% ================ User disable ================
if (~enable_cmd) && (~startup_active)
    shutdown_mode = true;
end

%% ================ Main state logic ================
if startup_active
    % -------- Startup blanking --------
    sw_state = false;
    gate_state = false;
    iref_state = 0.0;

elseif emg_mode
    % -------- Emergency shutdown --------
    gate_state = false;
    sw_state = false;
    iref_state = 0.0;
    blank_cnt = int32(0);

elseif shutdown_mode
    % -------- Controlled shutdown --------
    if iref_state > 0.0
        iref_state = iref_state - dI_down;
        if iref_state < 0.0
            iref_state = 0.0;
        end
    else
        iref_state = 0.0;
    end

    gate_state = false;

    if abs(Ibat) <= I_open_thresh
        sw_state = false;
    else
        sw_state = true;
    end

    blank_cnt = int32(0);

else
    % -------- Normal operation --------
    if enable_cmd
```

```
        % Wait until DC bus is healthy before allowing con-
nection
        if (Vdc >= Vdc_min_connect) && (Vdc < Vdc_max_warn)
            if bus_cnt < N_bus_stable
                bus_cnt = bus_cnt + int32(1);
            end
        else
            bus_cnt = int32(0);
        end

        if bus_cnt >= N_bus_stable
            sw_state = true;
            gate_state = true;

            % Soft limiting near normal max battery voltage
            if Vbat >= Vbat_max_normal
                iref_state = 0.0;
            else
                iref_state = Iref_in;
            end
        else
            sw_state = false;
            gate_state = false;
            iref_state = 0.0;
            blank_cnt = int32(0);
        end
    else
        sw_state = false;
        gate_state = false;
        iref_state = 0.0;
        blank_cnt = int32(0);
    end
end

%%    =================    Detect    switch    closing    edge
=================
% Start blanking timer only when switch changes 0 -> 1
if (~sw_prev) && sw_state
    blank_cnt = N_blank;
end

sw_prev = sw_state;

%%     =================     Normal     fault     detection
=================
% During startup blanking: ignore all faults
% During post-connect blanking: ignore only normal OV/OC
trips
if startup_active
    ovdc_cnt  = int32(0);
    ovbat_cnt = int32(0);
    ocbat_cnt = int32(0);
```

```
elseif blank_cnt > int32(0)
    blank_cnt = blank_cnt - int32(1);

    ovdc_cnt  = int32(0);
    ovbat_cnt = int32(0);
    ocbat_cnt = int32(0);

else
    % Battery terminal voltage exceeds normal negotiated
limit
    if Vbat > Vbat_max_normal
        ovbat_cnt = ovbat_cnt + int32(1);
    else
        ovbat_cnt = int32(0);
    end

    % DC bus warning/overvoltage region
    if Vdc > Vdc_max_warn
        ovdc_cnt = ovdc_cnt + int32(1);
    else
        ovdc_cnt = int32(0);
    end

    % Battery overcurrent
    if Ibat > Ibat_max_limit
        ocbat_cnt = ocbat_cnt + int32(1);
    else
        ocbat_cnt = int32(0);
    end

    if (ovbat_cnt >= N_fault) || (ovdc_cnt >= N_fault) ||
(ocbat_cnt >= N_fault)
        fault_lat = true;
        shutdown_mode = true;
    end
end

%% ================ Outputs ================
switch_cmd = double(sw_state);
gate_en = double(gate_state);
Iref_out = iref_state;
fault_latched = double(fault_lat);

if startup_active
    status = 6;  % startup blanking active
elseif emg_mode
    status = 4;  % emergency shutdown / fault latched
elseif shutdown_mode
    status = 3;  % controlled shutdown
elseif (blank_cnt > int32(0)) && sw_state
    status = 5;  % post-connect blanking active
elseif enable_cmd && (bus_cnt < N_bus_stable)
    status = 1;  % waiting for DC bus stabilization
```

```
elseif sw_state && gate_state
    status = 2;  % normal charging
else
    status = 0;  % idle
end
```